MODELING THE ELECTRODEPOSITION PROCESS OF COPPER ON COBALT CHROME

A Thesis by

Santosh Kumar Suggu

Bachelor of Technology, Amrita Vishwa Vidyapeetham, India, 2010

Submitted to the Department of Industrial and Manufacturing Engineering
and the faculty of the Graduate School of
Wichita State University
in partial fulfillment of
the requirements for the degree of
Master of Science

May 2014

**MODELING THE ELECTRODEPOSITION PROCESS OF
COPPER ON COBALT CHROME**

The following faculty members have examined the final copy of this thesis for form and content and recommend that it be accepted in partial fulfillment of the requirement for the degree of Master of Science with a major in Industrial Engineering

_____
Anil Mahapatro, Committee Chair

_____
Wilfredo Moscoso-Kingsley, Committee Member

_____
Visvakumar Aravinthan, Committee Member

ABSTRACT

A simulation is a computer program that helps in creating a real time abstract model of a process. Using simulations the costs of conducting experiments have come down and this has achieved flexibility in terms of optimizing parameters and durations. Electrodeposition is a process that uses electrical current to reduce dissolved metal cations from anode so that they form a metal coating on cathode. Electrodeposition is widely used for many applications varying from anti-corrosion coatings, decorative purposes to high precision nanotechnology cloaking devices. The objective of this research was to predict the electrodeposition of copper on cobalt chrome enabling an efficient optimization of the deposition. The main governing equation used for this model was mass species conservation. COMSOL, finite element software was used to solve the governing equations. The model was simulated to predict coating thickness under different conditions such as, varying current density, concentration and deposition durations. Experiments were conducted to validate the results from the simulation. Electrodeposition was carried in an electrochemical cell with Co- Cr as cathode and Cu as anode with $CuSO_4$ as an electrolyte. Coating thickness was determined using scanning electron microscope (SEM) and thickness gauge. There was an increasing trend in thickness in the both model and experiment when there was increase in current density. Decreasing trend was observed in the thickness in both model and experiment when there was reduction in the conductivity of the electrolyte. Model predicted results of the experiment at lower durations, at higher durations the experimental values deviated from the predicted values. These variations in the results were due to the limitations in the model and experimental verification methods, which could be worked in the future to reduce the variability.

TABLE OF CONTENTS

LIST OF TABLES

LIST OF SYMBOLS

c_i concentration of species, kg $/m^3$

D diffusivity, as a general reference

D_{AB} diffusivity of species A in species B, m^2/s

E_a activation energy, $J/mole$

F energy flux, W/m^2

h Planck's constant, $6.625 * 10^{-34} J.s$

k thermal conductivity, $W/m°C$

m mass, kg

M molecular weight, kg

$\dot{m}$ mass flow rate, kg/s

n flow behavior index, dimensionless

n order of reaction, dimensionless

$n_{A,z}$ mass flux of species A in the z direction, $kg/m^2.s$

r_A rate of generation of A per unit volume, kg of $A/m^3.s$

t time, s

T temperature; stress

u velocity in the x-direction, m/s

U thermal energy per unit volume, J/m^3

v velocity in y-direction, $\frac{m}{s}$

v_x, v_y, v_z velocities in x, y and z-directions respectively, m/s

V volume, m^3

X x-coordinate, m

X_a mole fraction of species A in liquid phase

α `thermal diffusivity, m^2/s

CHAPTER 1

INTRODUCTION

1.1   Background

Simulation modeling is the process used to create and analyze a digital prototype of a physical model to forecast not only its performance in the real world but also fluid flow and heat transfer patterns[1]. Simulation modeling helps designers and engineers to understand the ways and conditions, in which a part could fail, the loads it can withstand and helps to avoid recurring usage of physical prototypes to analyze designs for new and existing parts[2]. Users can practically investigate a number of digital prototypes before creating them. This technique is used for: optimizing geometry for weight and strength[3], selecting the material which meets the requirements of weight, strength, and budget [4] [5], simulating a part failure and finding the load conditions which caused it[6], estimating tolerable environmental conditions and loads that cannot be tested on physical prototypes[7], verifying hand calculations and validating the safety and survival of a physical prototype prior to testing[8].

Electrodeposition

It is a process which is used to reduce dissolved metal cations by using electrical current so that it forms a coherent metal coating on an electrode [9]. This process is mainly used to change the surface properties of a material. It is used for many technological applications, like automotive   industries,   electrical   industries,   corrosion   protection   of   metals   etc.

1.2   Motivation

Magnesium is an essential metal with vast uses and applications. It is ductile, light weight, denting and highest known damping capacity of any structural metal [10]. It can easily be welded, machined, forged and casted. Magnesium alloys are used in aerospace industry for manufacturing fuselages, engine parts, and wheels because of their weight advantage. Magnesium is desirable in surgical applications as it is bio-compatible, and it has a modulus of elasticity closer to bone [11] than currently used materials. Another major advantage of using magnesium as a surgical implant [12] is in its ability to biodegrade in the body. This means that the implant doesn't require any surgery to remove it. The main disadvantage of using Magnesium, it is very corrosive when exposed to air. Because of these applications in automotive [13], biological systems [14], many strategies to control corrosion is being studied. Electrodeposition is one of the techniques used for protection from corrosion. Modeling of electrodeposition of Magnesium is needed for optimizing the coating strategies.

1.3   Objective

The main objective was to model electrodeposition process to optimize the coating strategies of magnesium alloy which will be used for biodegradable metal implants. Since, Since Magnesium was corrosive in nature, inert substrate such as Copper and Cobalt Chrome system was chosen as a first step to model Magnesium. Copper was easy to electrodeposit and could easily be validated by conducting an electrodeposition experiment.

1.4   Thesis outline

This thesis was divided into five chapters. Chapter 2 presents the literature review of simulation and electrodeposition, their applications, advantages and limitations. It also included about modeling methodologies. Chapter 3 talked about the development of model to electroplate

copper on cobalt chrome. In Chapter 4, the materials and methodology of the modeling was explained. In Chapter 5, the results of simulation and experiment were discussed and in Chapter 6, Summary /Conclusion and future research directions were discussed.

CHAPTER 2

LITERATURE REVIEW

2.1   Electroplating

2.1.1   Introduction

Electroplating [15] or electro-deposition is a process which produces a dense, uniform, and adherent coating on a metal surface using electric current. Usually, the metal to be coated is the cathode and the anode can be one of the two: sacrificial anode (dissolvable anode) or permanent anode (inert anode).

2.1.2   Process

The metal to be coated is connected to the negative terminal and the sacrificial anode or permanent anode, i.e., metal to be deposited is connected to the positive terminal. Electrolyte in the electrochemical cell acts as a medium for the movement of electrons and forms the electric circuit between the electrodes (FIGURE 2.1).

Reduction reaction occurs at the cathode, where electrons move to cations in the electrolyte. The electrons at the cations migrate to the anode. The reactions in the electrochemical cell at the cathode follow the equation:
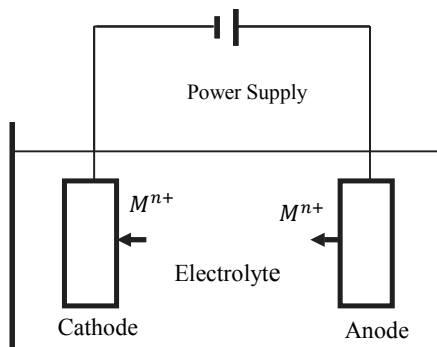

FIGURE 2.1. Principle of Electroplating

$$M^{n+} + ne^- \rightarrow M \quad (2.1)$$
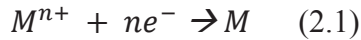
Oxidation reaction occurs at anode where electrons are supplied to the anions. The electrons move from anode to cathode. In the electrochemical cell, the anode reaction is:

$$M \rightarrow Mn^+ + ne^- \quad (2.2)$$
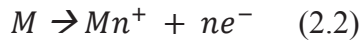
Prior to the electrodeposition process, the surface of the metal is treated to enhance the surface properties for a better coating.

Surface Preparation

Surface treatment is done to increase the corrosion resistance [16], minimize the friction on the surface [17], to reduce the wear to alter the physical properties like: conductivity [18], resistivity [19], change the texture of the surface like: color [20] and roughness [17] and to reduce the cost [21] of the finished product Surface treatment processes like polishing help in removing the machining defects, applying compressive stresses help in neutralizing the tensile stresses that have been applied.

For example, anodizing [22] is a passivation method done on the Aluminium components to change the thickness of the oxide layer. It helps in increasing the resistance towards corrosion, wear resistance, and improves better adhesion property of the metal [23].

Plating process

The electrodeposition process in carried out in a electrolytic cell. The electrolyte, also known as the plating bath, is prepared with aqueous salt containing positively charged ions of the metal to be plated on material. The metal material is immersed in the aqueous solution of the electrolyte and is attached to the negative end of the power source, which makes the metal material negatively charged cathode of the electrolyte, and the anode of the electrolyte is a metal rod of the metal to be plated on the metal material. This rod is attached to positive end of the

5

power supply. It is placed at the edge of the electrolyte. The electroplating process begins with the power source supplying the predetermined appropriate amount of circuit. At the same time, attraction between the metal material and the positively charged metal ions in the aqueous solution is caused by the negatively charged metal material cathode.

Thus, the metal ions in solution migrate to the negatively charged metal material and the metal ions are removed from the aqueous solution and directed onto the surface of the metal material. The next step is rinsing the metal material and post treating it to ensure that the plate surface is maintained.

2.1.3 Electroplating types

The electro-deposition processes are categorized to three major types based on the size and geometry of the job:

1. Direct Current Electro-deposition

2. Pulse Plating

3. Laser-Induced Metal Deposition

Direct Current Electro-deposition

In this type, the source of the current is the power from battery or rectifier. It converts alternating current electricity to regulated low-voltage DC current [24]. The dis-advantage of this process is that the geometric shape and contour of a work piece to be plated affect the thickness of the deposited layer. Usually, there would be a thicker deposition on the outside corners and thinner in the recessed areas of the work pieces with sharp corners and features. This un-equal deposition is due to the non-uniform DC current distribution. Therefore, to overcome the thickness irregularity effects, a placement of the anode(s) as well as modifications of the current density is required [25]. The advantages with this technique : the deposit is extremely hard and

wear resistant [26], it is a simple process with no complicated technology involved [27], and good corrosion resistance can be obtained in combination with nickel under plating [28]. Limitations of the process are: deposition rates are slow; needs multiple coatings [29], to obtain uniform thickness, machining is needed, susceptible to hydrogen embrittlement, exhibits brittleness, leading to micro-cracking and corrosion resistance is decreased over a period of time [30].

Pulse Plating

Pulse plating [31] is electro-deposition using pulsed currents, which can be unipolar (on–off) or bipolar (current reversal). Deposition of metal takes place in cathodic pulse duration with a bipolar pulse released. This kind of deposition which is repetitive and little re-dissolution enhances the topographical and physical properties of the coating [32]. The advantages of this technique: deposits with desired composition, structure, porosity and hydrogen content could be obtained by modifying pulse parameters [33], the additive requirement of plating process can be reduced by 50–60% in pulse plating process [34], this process eliminates thickness build up at high current density areas during current reversal [35] and also improves step coverage without pores reaching down to the substrate [36]. The limitations of this process are: the cost of a pulse rectifier is higher than a DC unit and is highly regulated and sophisticated design that is expensive to manufacture [37], one has to think and plan ahead with a series of procedures to follow in order to obtain the best results in this technology [38].

Laser-Induced Metal Deposition

A focused laser beam is used to accelerate the metal deposition in laser-induced metal deposition [31]. The deposition rate can be increased by 1000 times using this method [39]. The plating set up has a laser head with focusing optics and the electrochemical cell. On anode, the

focused laser beam is passed through a hole in the electrolyte and impacts the cathode surfaces. The advantages of the technique: the surface finish of the plated metal obtained by this method is better compared to other method [40]. The limitation of the method is setup being more expensive than other techniques[41] and for plating micro-electronic components this method is not preferred.

2.1.4 Applications of electroplating

Electroplating, also called electro-deposition has a wide range of applications in many industries. The surface to be plated could be either conductors (metals) or nonconductors (plastics). Electroplated products are used in automobile, ship, air space, machinery, electronics, jewelry, defense, and toy industries.

Automotive applications

Electroplating is widely used in automotive industry. Electroplating of Palladium [42] is used to manufacture catalytic converters because it has the ability to absorb excess hydrogen. Fasteners are electro-plated to have a better corrosive resistance.

Electrical Components

Majority of the electrical parts and components are used after electro-deposition process. Silver electroplating [43] has been used on copper or brass to enhance its conductivity and also used in silicon solar cells to increase its operating efficiency by 0.4%

2.1.5 Corrosion Protection

Electroplating is one of the techniques used to protect the metal from getting corroded. Nickel plating[44], tin plating and various alloys are used for corrosion protection on nuts, bolts, housings, brackets, other metal parts and components. Though expensive, gold electroplating provides not only corrosion, but also tarnish protection. For example, Magnesium was found to

be potential for biomedical applications; the problem being, it is corrosive in nature. So using electroplating, a protective layer on magnesium can be deposited to prevent it from corrosion.

2.2   Simulation Modeling

2.2.1   Introduction

Simulation is a tool used to evaluate the performance of a proposed system under study for duration of long periods of real time[45]. Simulation is performed under specific input conditions and output of the model is compared with that of the system. This is enabled by using simulation software. Physical processes that are being modeled can be understood by executing simulations. There are two types of simulation modeling, Stochastic[46] and Dynamic[47]. A stochastic model is performed from a source of randomness as it is based on certain assumptions of the system under study[48]. Statistical modeling is a stochastic model[49]. Examples of this type of modeling are linear regression[50], multiple regression[51], etc. Monte-Carlo method is a type of stochastic modeling[52]. Dynamic modeling[53] is performed using computer programs or software to evaluate complex systems. Simulation modeling used for optimizing material handling in a plant falls under this category[54].

2.2.2   Simulation of Electrodeposition

Modeling of electrodeposition using simulations helps in optimizing the coating strategies. Authors in the paper "Current Density Simulations in the Electrodeposition from Ionic Liquids: Effects of Conductivity" proved that alternative deposition methods other than CVD (Chemical Vapor Deposition), TBC (Thermal Barrier Coatings) were successful [55]. A simple galvanic cell was simulated using COMSOL Multiphysics. In the simulation model, they could successfully electrodeposit the metal on irregular shaped objects. Conductivity of ionic liquids was responsible for the current density distributions in the electrolyte. TBC specifications were

met in the case of simple electrode shape like disks, whereas the process was unsuccessful in case of complex objects like turbine blades. Absences of the coatings in critical places were successfully pointed out with the aid from simulations. Simulations results were almost similar in results with experimental electrodeposition [55].

Another important parameter which plays a vital role in for uniform surface coating is electrode spacing. In the paper "Parametric Modeling Study of Basic Electrodeposition in Microvias", authors modeled a coating process of microvias for the circuit boards. Loss of coating uniformity was observed when the electrode spacing decreased while greater electrode distance increased the uniformity of the coating[56]. The simulation results proved that, ideal distance value was must for best separation to obtain a uniform coating. It was also proved that, larger size of anode when compared to cathode resulted in a non-uniform coating. In theory, if the cathode and anode were of same height then the resultant deposition would be uniform, however the simulated model couldn't prove the results with the theoretical principles in this model. Similarly, movements of the ions in the electrolyte play a vital role in the formation of a good quality coating on the cathodic surface in the electrodeposition process. This was proved by the authors in the paper "Modeling the Electroplating of Hexavalent Chromium" [57]. The process of chromium plating was modeled in a 2D space using COMSOL Multiphysics. The simulation predicted that insufficient number of ions in the electrolyte would cause an uneven coating thickness and form voids on the coating surface. Individual impact of concentration and current density were the same with increased coating quality being obtained with increasing concentration / current density. However, varying both the parameters (concentration and current density) simultaneously did not result in an optimal coating. The simulation accurately predicted

conditions with high concentration and small current density as optimal conditions for obtaining best quality coating on the surfaces.

Another study by Wei and coworkers showed that electrolyte additives was an important parameter in the electrodeposition of the metal [58]. They numerically modeled copper deposition in a trench shaped structure [58]. Electrolyte additives affected the exchange current density of the electrolyte and the over potential of the electrodeposition. Results from the simulation proved that both velocity and over potential decreased with decrease in the additive concentration. However, the effect of additive was more pronounced at the top of the trench as compared to the bottom surface of the trench.

Using PHYSICA, a multi physics solver software authors modeled an electrodeposition process in the paper "Multiphysics Modeling of the Electrodeposition Process" to demonstrate that electrode kinetics played an important role in the electrodeposition process [59]. Electrode kinetics defined the deposition process using the rate determining step and current distributions. Simulation results proved that variables like surface electrode potential and the ion concentration in the electrolyte also influenced the kinetics associated with the deposition process. Along with the above variables, it also explained the importance of the interfaces of the model and moving boundary conditions. The simulation model demonstrated the importance of the interface and boundary selection on the electrodeposition process. Appropriate selection of these parameters was needed for accurate prediction when compared with experimental results.

Simulation of the electrodeposition process for a micro device fabrication in a trench shaped electrochemical cell showed that limitations on the diffusion transport growth of ions caused non-uniformity of the coatings formed [60]. Authors proved that the diffusion of ions was based on the shape of the electrolytic cell and the electrolyte in the shaped structure (trench)

11

usually remained stagnant causing variations in the deposition. In these shaped (trench) structures the model predicted uneven deposition due to the effects of the diffusion limits causing the coating surface to be roughened and subsequently becoming unstable when the rate of deposition was increased. Changes in electrode surface chemistry such as hydrogen evolution could also complicate the deposition process [60].

2.2.3 Advantages of Computer Simulation

1. **Value.** Simulation model assists in better investment [61]. For example, a simulation model used in a production shop floor reduces waiting time which increases the productivity. This is one of the biggest advantages of using a simulation model.

2. **Time.** A simulation model studies the significance of a process or design change faster than it is done in the real world system [62]. For example, the arrival rate of a component in a process can be easily understood from a simulation then actually waiting for it to be recorded in a real time process, thus saving a lot of time.

3. **Accuracy.** Simulation models provide the accuracy that is not provided by computational mathematic algorithms[63]. For example, certain numerical required for a production system to function is accurately measured by simulation modeling techniques.

4. **Visibility.** A simulation model aids in visualizing results so that the results attained during the experiment can be conveyed more efficiently[64]. For example, graphically we can obtain the results which aid in better understanding the problem.

5. **Versatility.** Simulation modeling [65] can be used in a number of fields, such as finance, logistics, manufacturing, health care, etc. This is one of the biggest advantages of simulation modeling.

2.2.4   Limitations of Computer Simulation

1. Large-scale-manufacturing systems are very complex. Writing computer programs to model such systems can be a very expensive task. Even under best circumstances simulation projects consume a lot of time, frequently requiring many months before obtaining valid results.

2. Complex simulation models require extensive computer time which is costly exercise. This limits the designer's freedom to generate alternative designs.

3. Pseudo-data that detail the conceived system to imitate the real system must be provided to simulation model. The data regarding the processing demand information and operation rules are not available in the design phase.

4. In some cases where problem is not clearly defined, a simulation project always contains a risk factor which neither the designer nor the user of the model can find out in the early stages of design project.

2.3   Modeling problem formulation

2.3.1   Introduction

Simulation modeling software is used to model a real system under study using mathematical formulae. The correlation between the model and the real system is compared. A few changes are made if the correlation is not true. It is applied in chemical reactions, power reactors, control systems, electroplating, etc. Algorithms can also be used to simulate models. Software used in industrial applications are ARENA [66], COMSOL [67], ASCEND [68] etc. These models are based on the fundamental laws and governing equations like mass transfer, heat transfer. These can be solved using the solvers in the simulation software.

2.3.2 Methodology

The process of the modeling software is divided into three parts – preprocessing, processing and post processing.

Preprocessing:

Input of the required data should be provided in this step. It addresses two primary concerns: Identifying the objectives and methods to resolve them.

1. Identifying the Objectives:

    i. Geometry: The computational domain for the problem is entered in the software.

    ii. Governing equations: A set of mathematical equations describing the physical problem is chosen.

    iii. Boundary conditions: The appropriate boundary conditions, with respect to each governing equation to be solved, are entered.

    iv. Initial conditions: The initial conditions for the problem are defined.

    v. Properties: The material properties, such as, thermal conductivity, density, etc. are specified.

2. Methods to resolve the objectives:

    i. Meshing: The computational domain is divided into number of small elements, to solve the governing equations numerically.

    ii. Time steps: Here it is verified that if the problem is time- dependent. The time over which the problem has to be solved and the time step increment to be used by the solver are specified.

iii.   Solving algebraic equations: Appropriate software is chosen to solve the set of algebraic equations from the original partial differential equations in processing stage.

iv.   Tolerances: Tolerances are specified in the CAE software for error correction.

Processing:

Processing is automated based on the parameters provided in preprocessing. This stage involves conversion of partial differential equations into algebraic equations in order to obtain the values of temperature, velocity, concentration, etc.
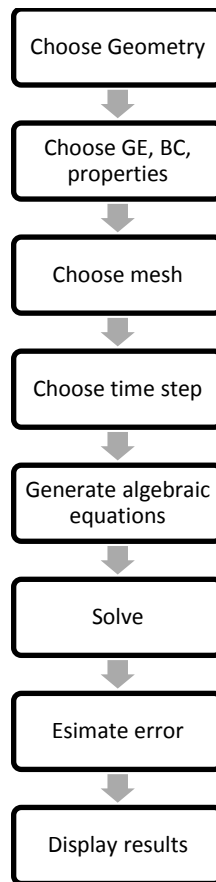

FIGURE 2.2 . Flow chart for model development and solution, showing steps for preprocessing, processing and postprocessing [69]

Post Processing:

The solutions obtained from the previous step are visualized using graphs, histograms and animations.

2.3.3 Modeling Software

There is variety of computer software packages available for modeling. Some of them are Arena, AutoCAST [70], COMSOL Multiphysics [71], Hyper Works, MATLAB [72], NEi Nastran etc. For the current study, COMSOL Multiphysics software was used to model the problem.

2.4 COMSOL

COMSOL is an algorithm used to resolve the governing equations and boundary conditions using finite-element method (FEM) [67].The software can simulate different physics by solving the corresponding equations such as, heat transfer, mass transfer, electrochemistry, fluid flow, electromagnetics and solid mechanics. One dimensional, 2D, axisymmetric & 3D steady state or transient simulations axisymmetric in complex geometry can be analyzed through COMSOL.

2.4.1 Problem Formulation

Problem formulation involves creating an equivalent mathematical formulation of a physical problem, i.e., finding equations which describe the physical processes that constitute the problem which virtually replaces the process. For example, consider electrodeposition of a metal A over metal B. Metal ions from a diffuse through the electrolyte and gets deposited on B. The system is an equivalent to a mass transfer, as material is moving from one point to another. In this, we would find out the thickness of the deposited layer over time which provides the time

taken to deposit required thickness. Simulation requires describing the physical process in mathematical form in order to develop a formulation.

The mathematical analog comprise of geometric parameters defined under objectives section in processing stage , i.e., computational domain, governing equation, boundary conditions, material properties and other parameters that define the real process. The computations are performed on the domain while the governing equations depict the conservation of mass species and boundary conditions are the constraints defined by the domain environment.

2.4.2 Steps Involved

Obtaining mathematical formulation is divided into several steps. First, we must decide on the final goal of the simulation followed by the selection of appropriate simulation region subsequently the governing equations and boundary conditions that define the process. Different material properties and parameters relevant to the situation must be provided to address the issues of specific cases.
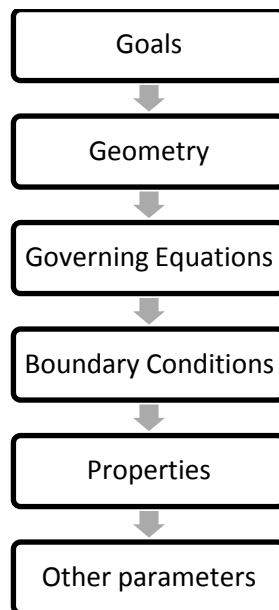

FIGURE 2.3 Steps in problem formulation [69]

In order to simplify the model complexity to achieve complex possible formulation, we start with simple 2D geometry without heat transfer and involving only constant properties of temperature or concentration, etc. Important results obtained by this include:

1. Regions to be included

2. Proportions of large regions to be considered.

3. Number of dimensions

4. Symmetry to reduce the domain.

Problems that involve multiple regions such as a solid and liquid or two solids are not included unless required. Depending on the physical process complete fluid area can be considered with solid as a boundary. The equations which are not applicable to the considered region(s) are not solved.

The computation memory and time required are the function of computational domain. Computation time varies disproportionately with the number of nodes and the proportions of larger domain to be included must be investigated with attention. The designed computation then determines the appropriate domain size.

The required dimensions are chosen based on the greatest number of changes in the variables of interest. The central purpose of introducing symmetry into the model is to minimize the computation by minimizing the domain size. Fig. 2.4 shows provides examples of reduced domains
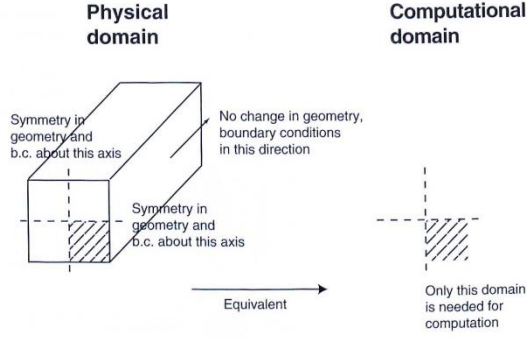
FIGURE 2.4 Reduction of geometry using symmetry [69]

2.4.3 Governing Equations

The three most distinct equations of physics are fluid flow, heat transfer and mass transfer. Depending on the problem we use the equation(s). The governing equations are always used in simplified form. The equations for mass conservation, momentum conservation, energy conservation and mass species conservation are described below.

The Total mass conservation (continuity equation) is defines as:

$$\frac{\partial \rho}{\partial t} + \frac{\partial}{\partial x}(\rho v_x) + \frac{\partial}{\partial y}(\rho v_y) + \frac{\partial}{\partial z}(\rho v_z) = 0 \quad (2.3)$$

Momentum conservation equations (fluid flow equations)

$$\rho \frac{\partial v_x}{\partial t} + \rho \left(v_x \frac{\partial v_x}{\partial x} + v_y \frac{\partial v_x}{\partial y} + v_z \frac{\partial v_x}{\partial z} \right) = -\frac{\partial \rho}{\partial x} + \mu \left(\frac{\partial^2 v_x}{\partial x^2} + \frac{\partial^2 v_x}{\partial y^2} + \frac{\partial^2 v_x}{\partial z^2} \right) + \rho g_x \qquad (2.4)$$

$$\rho \frac{\partial v_y}{\partial t} + \rho \left(v_x \frac{\partial v_y}{\partial x} + v_y \frac{\partial v_y}{\partial y} + v_z \frac{\partial v_y}{\partial z} \right) = -\frac{\partial \rho}{\partial y} + \mu \left(\frac{\partial^2 v_y}{\partial x^2} + \frac{\partial^2 v_y}{\partial y^2} + \frac{\partial^2 v_y}{\partial z^2} \right) + \rho g_y \qquad (2.5)$$

$$\rho \frac{\partial v_z}{\partial t} + \rho \left(v_x \frac{\partial v_z}{\partial x} + v_y \frac{\partial v_z}{\partial y} + v_z \frac{\partial v_z}{\partial z} \right) = -\frac{\partial \rho}{\partial z} + \mu \left(\frac{\partial^2 v_z}{\partial x^2} + \frac{\partial^2 v_z}{\partial y^2} + \frac{\partial^2 v_z}{\partial z^2} \right) + \rho g_z \qquad (2.6)$$

Energy conservation equation (heat transfer equation)

$$\rho C_p \frac{\partial T}{\partial t} + \rho C_p \left(v_x \frac{\partial T}{\partial x} + v_y \frac{\partial T}{\partial y} + v_z \frac{\partial T}{\partial z} \right) = k \left(\frac{\partial^2 T}{\partial x^2} + \frac{\partial^2 T}{\partial y^2} + \frac{\partial^2 T}{\partial z^2} \right) + Q \quad (2.7)$$

Mass species conservation equation (mass transfer equation)

$$\frac{\partial c_A}{\partial t} + \left(v_x \frac{\partial c_A}{\partial x} + v_y \frac{\partial c_A}{\partial y} + v_z \frac{\partial c_A}{\partial z} \right) = D_{AB} \left(\frac{\partial^2 c_A}{\partial x^2} + \frac{\partial^2 c_A}{\partial y^2} + \frac{\partial^2 c_A}{\partial z^2} \right) + R_A \quad (2.8)$$

The transient, convection, diffusion and generation terms in the governing equations are used based on the process and its factors.

Transient: Transient means dynamic in nature. The transient term ($\frac{\partial c_A}{\partial t}$) denotes the rate of change of storage. The term should be considered if the process changes significantly or ignored if the process remains steady for most of the time.

Convection: The convection term, mathematically defined as $\left(v_x \frac{\partial c_A}{\partial x} + v_y \frac{\partial c_A}{\partial y} + v_z \frac{\partial c_A}{\partial z} \right)$ with respect to heat or mass transfer equation, represents the transport of energy or species due to bulk flow. The term should be considered when the domain is fluid and ignored in a solid region with no bulk flow, as it would be non-porous medium.

Diffusion: The diffusion term ($D_{AB} \left(\frac{\partial^2 c_A}{\partial x^2} + \frac{\partial^2 c_A}{\partial y^2} + \frac{\partial^2 c_A}{\partial z^2} \right)$) represents the contribution to energy transport from conduction or diffusion to retain when qualitative information suggests that diffusion is likely to take place most of the time. this term may be ignored when (1) uniform and rapid heat generation where the boundaries are insulated, for temperature gradient not to develop; (2) the equation is used only as an analog and there is no real species to diffuse;(3) diffusion is negligible for a large species such as bacterium.

Generation: The generation term (R_A) known as source term whose negative value represents depletion, called as sink term. In case of heat transfer, the term represents conversion of generated heat into other forms of energy such as electromagnetic, ultrasonic or various other modes of heating. The term is ignored when the generated heat is much less than transported energy while in the mass transfer; it denotes formation of chemical species. The negative value is because of conversion of species into other forms

2.4.4 Boundary and Initial Conditions

Six boundary constraints are defined for 3D, four at four edges for 2D and two for 1D at two points on the line. Usually one boundary condition is specified at the surface and parameters like process changing with time, non-uniform distribution of temperature, material are specified at the start of simulation.

CHAPTER 3

DEVELOPMENT OF MODEL

3.1   Simulation Model

The objective was to mathematically model the electroplating of Copper on Colbalt Chrome in copper sulphate electrolyte. This model was set as a 2D time dependent model using Secondary Current Distribution, Electrochemistry using COMSOL. The Nernst Planck Equation governed the ionic mass transport process that occured in the electrolyte. The Nernst- Planck Equation is a conservation of mass equation and is extension of Fick's Law of Diffusion[73] to include electrostatic forces.

The deposition at cathode and the dissolving of the anode was taken place at 100% current yield. During the process, the change in the electrolytic density in the electrochemical cell occured and the change in the density at anode was more than cathode. This induced free convection in the cell. Under the assumption that the variation in composition is small, free convection component was neglected. The process was assumed to be time dependent as the boundary of the cathode was moving as the deposition of the metal was taking place. The model is governed by mass conservation for the copper ions Cu^{2+} and sulphate SO_4^{-2} and the electroneutrality condition.

The model geometry is shown in FIGURE 3.1 below. The upper boundary represented anode, and cathode was placed at the bottom. The vertical walls were assumed to be insulated.
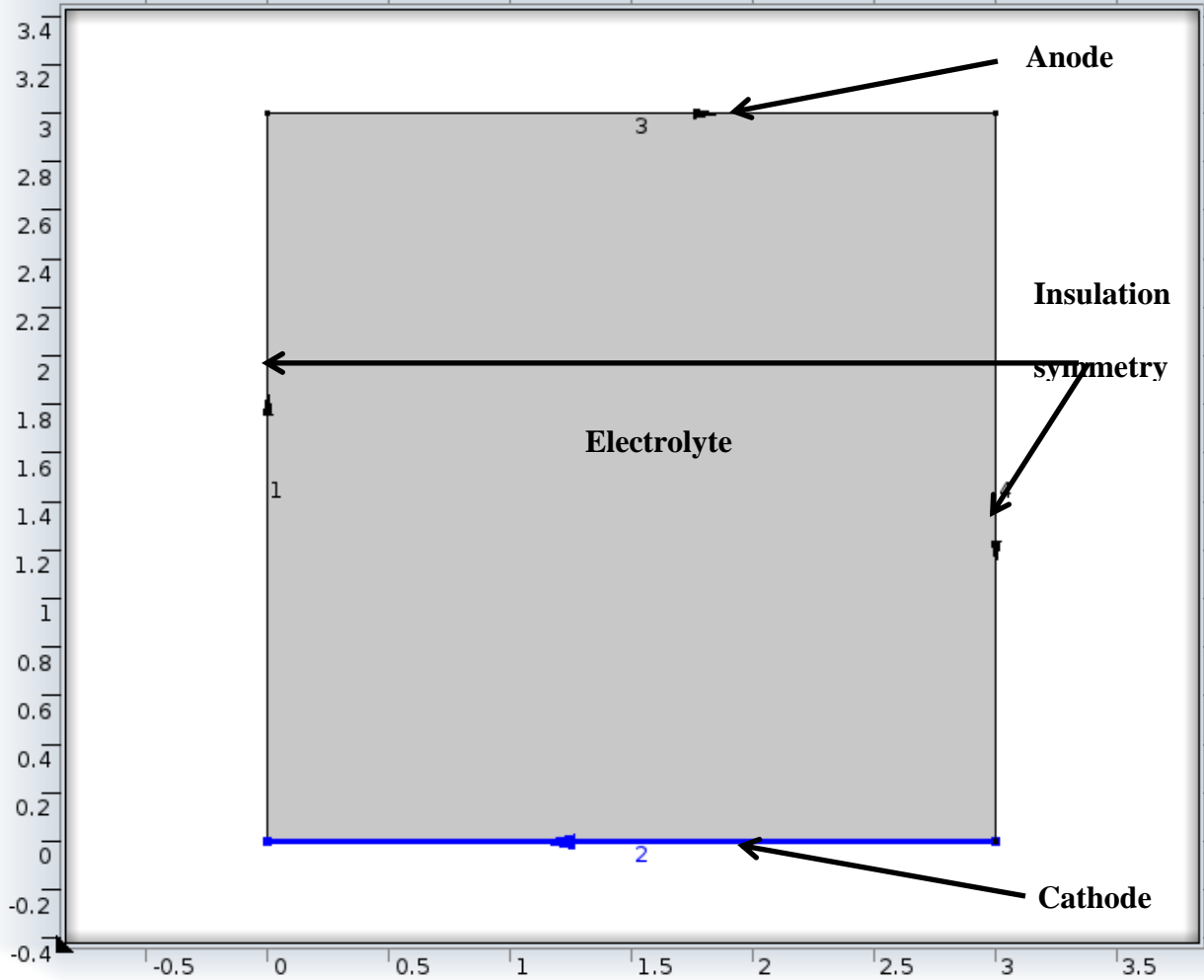
FIGURE 3.1. Geometry of the model

3.2 Assumptions

The assumptions were as follows:

1. Dilute solution theory[74]. This states that there were negligible interactions between the solute species.

2. The Nernst Einstein equation, $D_i = u_i RT$, which is implicit in the infinite dilute solution theory [75]

3. The current density distribution was assumed to be uniform on the surface of the electrode.

4. The current density took the form of Butler-Volmer equation[76], which expressed the dependence of the current on the composition of the electrolyte solution adjacent to the electrode surface and on the relative activity of the solid state species and the exponential dependence of the current on the over potential

5. The physical, transport and kinetic parameters [77] were constant throughout the solution.

6. Solution was isothermal [78].

7. No homogeneous chemical reactions occurred in the electrolyte

3.3   Governing Equations

The transport equation which was applied in the diffusion layer was based on the flux equation of the ionic species in the solution. Mass transport in the solution occurred because of migration in electric field, diffusion in concentration gradient and convection in the flow field. The general mass balance equation is given below

$$N_i = -z_i u_i F c_i \nabla \emptyset_l - D_i \nabla c_i + V_i c_i \qquad (3.1)$$

The flux equations explaining the behavior of electrochemical systems are related to the Second Law of Thermodynamics[79]. Consider two neighboring volume elements V' and V'' of a solution that have same temperature and pressure but different electrochemical potentials of their constituents. The difference between the electrochemical potential of species i, $\tilde{\mu}'_i$ and $\tilde{\mu}''_i$, in these volume elements implies that this species tends to move from one volume element to the other as there is no distribution equilibrium. This motion of species i from one volume element to its neighbor is generically called transport of species i. As the transport of the different species in solution takes place under thermal and mechanical equilibrium, the change in internal energy U of these two volume elements is

$$dU' = TdS' + \sum_i \tilde{\mu}'_i dn'_i \qquad (3.2)$$

$$dU'' = TdS'' + \sum_i \tilde{\mu}''_i d''_i \qquad (3.3)$$

Where T is the thermodynamic temperature, S is the entropy and n_i the number of moles of species i. Considering the exchange of matter between V' and V'', which takes place without energy exchange with their surroundings, it is satisfied that

$$T(dS' + dS'') = \sum_i (\tilde{\mu}''_i - \tilde{\mu}'_i)dn'_i \geq 0 \qquad (3.4)$$

Each individual term of the sum is positive when the transport of species i is not coupled to transport of other species. In this case, dn'_i is determined only by $(\tilde{\mu}''_i - \tilde{\mu}'_i)$ and species i moves towards the region in which its electrochemical potential is lower, that is, $dn'_i < 0$ when $\tilde{\mu}''_i < \tilde{\mu}'_i$ and vice versa. For example, this takes place in the case of ionic species in diluted solutions. When the transport of different species is coupled, one or more terms in the sum could be negative, but the sum is always positive.

The transport of the species i is described in terms of either its velocity $\vec{V_i}$ or its flux density $\vec{J_i} = c_i \vec{V_i}$. If the area of the surface between the two volume elements is dA and its orientation is given by the unit vector $\hat{n}$ (from V' to V''), the number of moles of species i crossing the surface in a time dt is $dn'_i = -\vec{J_i}\hat{n}\, dAdt$.

When the difference between $\tilde{\mu}''_i$ and $\tilde{\mu}'_i$ is not very large, it can be assumed that the rate of change of the amount of species $i, dn'_i/dt$, is proportional to the difference $\tilde{\mu}''_i - \tilde{\mu}'_i$ or to the gradient of this potential normal to the surface, $\partial \tilde{\mu}_i/\partial n \equiv \vec{\nabla}\tilde{\mu}_i\hat{n}$. The velocity of species i in linear approximation is expressed as

$$\vec{V_i} = -u_i \vec{\nabla}\tilde{\mu}_i \qquad (3.5)$$

Where u_i is its mobility

Flux density takes the form

$$\vec{J_i} = c_i\vec{V_i} = -u_i c_i \vec{\nabla}\tilde{\mu}_i = -\frac{D_i c_i}{RT}\vec{\nabla}\tilde{\mu}_i \tag{3.6}$$

Where R is the universal gas constant and the Einstein relation between mobility and diffusion coefficient, $D_i = u_i RT$, has been used.

At constant temperature and pressure, the gradient $\vec{\nabla}\tilde{\mu}_i$ is caused by the changes in composition and electrical potential ø so that

$$\vec{\nabla}\tilde{\mu}_i = RT\vec{\nabla}\ln c_i + z_i F\vec{\nabla}\emptyset_l \tag{3.7}$$

Where F is the Faraday constant and z_i is the charge number of species i. Taking Eq. (3.7) to Eq. (3.6), the Nernst-Planck flux equation

$$N_i = -D_i(\vec{\nabla}c_i + z_i c_i f\vec{\nabla}\emptyset_l) \tag{3.8}$$

is obtained, where f denotes the ratio F/RT. The terms in the righthand side of this equation represent the transport mechanisms of diffusion and migration, respectively. Diffusion is a consequence of the random thermal motion of the particles which makes the concentration of all species uniform. Migration causes the influence of the electric field, $\vec{E} = -\vec{\nabla}\emptyset_l$, on the random motion of the charged particles, and Eq.(3.8) shows that the particles a component of their velocity along the direction of the electric field as a result of this influence.

Flux of species i due to bulk flow in a moving fluid in X-direction,

$$(F_x) = u_i c_i \tag{3.9}$$

Therefore, the flux expression for each species i can be written as

$$N_i = -z_i u_i F c_i \nabla\emptyset_l - D_i \nabla c_i + V_i c_i \tag{3.10}$$

Where the ionic mobility u_i, is assumed to be related to the diffusion coefficient D_i by the Nernst-Einstein equation[80]

The material balance equation for each ionic species at every point within the diffusion layer is as follows

$$\frac{\partial c_i}{\partial t} = -\nabla . N_i + R_i \qquad (3.11)$$

Where R_i is the production rate of species i due to homogeneous chemical reactions

Under the assumption, variations in composition are negligible in the electrolyte and migration of ions gives the net contribution to current in the electrolyte equation

The concentration gradients in the above equations are neglected in the Secondary Current deposition interface and the current density is obtained from Ohm's law

$$i_d = -\sigma_l \nabla \phi_l \qquad (3.12)$$

Where σ_l denotes the electrolyte conductivity.

Since the electrolyte composition is assumed to be constant, the material balances are unsolved for the Secondary current distribution,

The electroneutrality condition is given by the following expression:

$$\sum_{i=0}^{n} z_i c_i = 0 \qquad (3.13)$$

Boundary conditions for the anode and the cathode were given by the Butler-Volmer equation for the copper deposition(detailed explaination of the equation were discussed in Sec 3.4.8).

3.4   Electrode Kinetics

Consider the reaction given below:

$$A \leftrightarrow B \qquad (3.14)$$

K_f and K_b are the rate constants of the forward and backward reactions respectively.

3.4.1   Reaction Rates:

The reaction rate, also known as rate of reaction or speed of reaction, for a reactant or product in a particular reaction is defined as how fast or slow a reaction occurs.

The rate of forward reaction can be calculated by: $R_f = k_f C_A$ \qquad (3.15)

The rate of backward reaction can be calculated by: $R_b = k_b C_B$ \qquad (3.16)

The net rate of reaction can be calculated by: $R_{net} = R_f - R_b$ (3.17)

From equations (3.15) and (3.16)

Thu: $R_{net} = k_f C_A - k_b C_B$ (3.18)

3.4.2 Equilibrium

Equilibrium is point at which the net reaction rate is zero. From the above equations, we can obtain the equilibrium concentration ratio as follows

$$\frac{k_f}{k_b} = K = \frac{C_B}{C_A}$$ (3.19)

Where K is the equilibrium constant (K)

Rate constant vary with temperature, generally it increases with T. The rate constant (K) and temperature are related by:

$$K = Ae^{(-E_a/RT)}$$ (3.20)

Where, E_a=activation energy, R=gas constant and A=pre exponential factor

3.4.3 Activation energy

Activation energy[81] is the barrier that has to be overcome by the reactants before they are converted to product. More energy is required by the reactants when there is a larger barrier for the activation energy.

$$K = Ae^{(-E_a/RT)}$$ (3.21)

a. Exponent term $e^{(-E_a/RT)}$ is a probabilistic feature of the energy barrier component which has to crossed

b. Pre exponential factor A, also known as frequency factor, gives a number of times the attempt was made to overcome the energy barrier

c. Consider the electrode reaction: $O + ne = R$ (3.22)

28

Where k_f and k_b are the forward and backward reaction rate constants respectively. This is a general redox reaction, where O represents oxidized state and R represents reduced state. For this reaction, the equilibrium state is governed by the Nernst equation, which relates the equilibrium potential of the electrode (E_{eq}) to the concentration of the reactants and products (O and R)

$$E_{eq} = E^0 - RT/nF[ln(\frac{C_R}{C_o})] \qquad (3.23)$$

3.4.4 Overvoltage

A given current will require a penalty that should be paid in terms of electrode potential-penalty called overvoltage[82] due to irreversibility.

$$\eta = E_{eq} - E \qquad (3.24)$$

E_{eq} is the expected electrode potential and E is the electrode potential

$$\eta = a + b \log i \qquad (3.25)$$

Where a and b are constants and I is the current density. This is the Tafel equation.

3.4.5 Kinetics of electrode reactions

Rates of forward and backward reaction

$$O + ne = R \qquad (3.26)$$

For the above reaction, the rate of the forward reaction is given by:

$$R_f = k_f \, C_o(0,t) = i_c/nF \qquad (3.27)$$

Where $C_o(0,t)$ is the surface concentration of O.

Rate of the backward reaction is given by:

$$R_b = K_b \, C_R(0,t) = i_a/nF \qquad (3.28)$$

Reaction rate and current are correlated. Reduction occurs at the cathode and oxidation at the anode.

Net reaction rate

The net reaction rate or net current is given by

$$R_{net} = R_f - R_b = \frac{i}{nF} = \frac{i_c - i_a}{nF} = [k_f\ C_o(0,t) - k_b\ C_R(0,t)] \qquad (3.29)$$

3.4.6 Potential dependence of k_f and k_b

Both k_f and k_b are potential dependent functions

The forward reaction, which is a reduction, is an electron accepting process. The rate of reaction increases when the electrode potential reaches higher negative because the electrode loses electrons more easily. The opposite happens in the backward reaction, i.e., oxidation reaction.

At equilibrium

The electrode potential and oxidation and reduction concentrations make net reaction rate zero. Then :

$$i_c = i_a;\ R_f - R_b \qquad (3.30)$$

It can also be written as:

$$k_f\ C_o(0,t) = k_b\ C_R(0,t) \qquad (3.31)$$

$$ln(k_b) - ln(k_f) = ln[\frac{C_o(0,t)}{C_R(0,t)}] \qquad (3.32)$$

Therefore calling in the Nernst equation:

$$ln(k_b) - ln(k_f) = ln[\frac{C_o(0,t)}{C_R(0,t)}] = F/RT(E - E^\circ) \qquad (3.33)$$

Upon differentiating the above equation with respect to E, we get:

$$RT/F[\frac{\partial\{ln(k_b)\}}{\partial E} + [\frac{\partial\{ln(1/k_f)\}}{\partial E}] = 1 \qquad (3.34)$$

$$1 - \alpha\ +\ \alpha\ \ \ = 1 \qquad (3.35)$$

The terms on the left hand side of the reaction sum up to 1 and called symmetry factors (for one electron transfer in the reaction).

3.4.7 Reductive and Oxidative symmetry factors

The reductive symmetry factor is associated with the forward reaction which is represented by α

$$RT/F[\frac{\partial\{ln(1/k_f)\}}{\partial E}] = \alpha \qquad (3.36)$$

The oxidative symmetry factor therefore becomes $(1 - \alpha)$

$$RT/F[\frac{\partial\{ln(k_b)\}}{\partial E}] = 1 - \alpha \qquad (3.37)$$

The term α is the measure of the symmetry of energy barrier. If the change in the potential is same on both sides of the barrier, then α=0.5=1- α. Any asymmetry in the change causes fractional values of α.

Standard rate constants

$$ln(\frac{1}{k_f}) = \alpha FE/RT + c \qquad (3.38)$$

If, $k_f = k_f°$, then E=E°

$$k_f = k_f°e^{\{-[\frac{\alpha F}{RT}](E-E°)\}} \qquad (3.39\text{-a})$$

Similarly:

$$k_b = k_b° e^{\{-[\frac{\alpha F}{RT}](E-E°)\}} \qquad (3.39\text{-b})$$

$k_f°$ and $k_b°$ are termed as standard rate constants

If the concentrations of oxidation and reductions are same, and the potential is maintained at E° to cause any current flow:

From above equation, $k_f° = k_b°$

The larger the value of K°, the faster is the equilibrium. Reactions with small standard rate constants are slow. The standard rate constant is large for simple redox couples

3.4.8 The Butler-Volmer Theory

$$i = nF\, k^\circ[C_o(0,t)e^{\left\{-\left[\frac{\alpha nF}{RT}\right](E-E^\circ)\right\}} - C_R(0,t)\, e^{\left\{-\left[\frac{(1-\alpha)nF}{RT}\right](E-E^\circ)\right\}}]$$ (3.40)

Where n is the number of electrons transferred. This is the Butler –Volmer[76] formulation of electrode kinetics. There are two components, of current i.e., anodic and cathodic, and it is exponentially dependent on potential. The net reaction rate is given by:

$$R_{net} = i/nF = [\,k_f\, C_o(0,t) - \, k_b\, C_R(0,t)]$$ (3.41)

$$i = nF[k_f\, C_o(0,t) - \, k_b\, C_R(0,t)]$$ (3.42)

Substituting the values for k_f and k_b

$$i = nF\, k^\circ[C_o(0,t)e^{\left\{-\left[\frac{\alpha nF}{RT}\right](E-E^\circ)\right\}} - C_R(0,t)e^{\left\{-\left[\frac{(1-\alpha)nF}{RT}\right](E-E^\circ)\right\}}]$$ (3.43)

This formulation is called the Butler –Volmer formulation of electrode kinetics

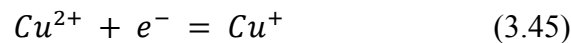**At Equilibrium**

$$C_o(0,t) - \, C_R(0,t)\, e^{\left\{\left[\frac{nF}{RT}\right](E-E^\circ)\right\}} = \left[\frac{i}{nF}k^\circ\right]\left[e^{\left\{\left[\frac{\alpha nF}{RT}\right](E-E^\circ)\right\}}\right]$$ (3.44)

At equilibrium, $i = 0$

3.5 Equations Involved

The deposition process is assumed to take place through the following simplified mechanism:

$$Cu^{2+} + e^- = Cu^+$$ (3.45)

$$Cu^+ + e^- = Cu$$ (3.46)

The first step is rate determining step (RDS), and the second step is assumed to be at equilibrium, which gives the following relation for the local current density as a function of potential and copper concentration:

$$i_{ct} = i_0[\exp\left(\frac{1.5Fn}{RT}\right) - \frac{c_{Cu^{2+}}}{c_{Cu^{2+},ref}}\exp\left(-\frac{0.5Fn}{RT}\right)]$$ (3.47)

where n denotes the over potential defined as

$$n = \emptyset_{s,0} - \emptyset_1 - \Delta\emptyset_{eq} \tag{3.48}$$

where $\emptyset_{s,0}$ denotes the electronic potential of the respective electrode.

Equation at the cathode is given by:

$$N_{Cu^{2+}}.\boldsymbol{n} = -\frac{i_0}{2F}\left[\exp\left(\frac{1.5F(\emptyset_{s,cat}-\emptyset_1-\Delta\emptyset_{eq})}{RT}\right)\right] - \frac{c_{Cu^{2+}}}{c_{Cu^{2+},ref}}\exp\left(-\frac{0.5F(\emptyset_{s,cat}-\emptyset_1-\Delta\emptyset_{eq})}{RT}\right)] \tag{3.49}$$

where **n** denotes the normal vector to the boundary.

Equation at the anode is

$$N_{Cu^{2+}}.\boldsymbol{n} = -\frac{i_0}{2F}\left[\exp\left(\frac{1.5F(\emptyset_{s,an}-\emptyset_1-\Delta\emptyset_{eq})}{RT}\right)\right] - \frac{c_{Cu^{2+}}}{c_{Cu^{2+},ref}}\exp\left(-\frac{0.5F(\emptyset_{s,an}-\emptyset_1-\Delta\emptyset_{eq})}{RT}\right)] \tag{3.50}$$

The amount of deposition is understood by the Faraday's laws of electrolysis [83] which states that the amount of a material deposited on an electrode is proportional to the amount of electricity used. For reduction of one mole of a given metal ion (charge of n^+), n moles of electrons are used for reduction. The total cathodic charge for the coating , Q(C), is the product of the number of gram moles of the metal coated, m, and the number of electrons required for the reduction reaction, n, Avogadro's number, N_a (number of atoms in a molecule), and the electrical charge per electron, Qe(C). Thus, charge required to reduce m moles of metal is given by

$$Q = mnN_aQe \tag{3.51}$$

The product of Avogadro's number, N_a (the number of atoms in a mole), and the electrical charge per electron, Qe(C) gives the Faraday constant, F. The number of moles of the metal reduced by charge Q is:

$$m = Q/nF \tag{3.52}$$

The total charge used in the deposition can be calculated by the product of the current, I (A), and the time of deposition, t (sec), where the deposition current is constant. When current varies with time during the deposition process, Q can be calculated by,

$$Q = \int I \, dt \qquad (3.53)$$

The weight of the deposit, W(g), can be calculated by product of the number of moles of metal reduced and atomic weight, Mw, of the deposited metal is given by:

$$W = \frac{Mw}{nF} \int I \, dt \qquad (3.54)$$

The thickness of the deposition, d (cm), can be solved by:

$$d = \frac{W}{\rho A} = \frac{Mw}{nF\rho A} \int I \, dt \qquad (3.55)$$

Where ρ is the density of the metal (g=cm^3) and A is the area of deposition (cm^2).

3.6 Boundary Conditions

All boundaries (B1 and B4) were insulating:

$$N_{Cu^{2+}} . n = 0 \qquad (3.56)$$

3.7 Initial Conditions

The initial conditions of the electrolyte were:

$$c_{Cu^{2+}} = c_0 \qquad (3.57)$$

CHAPTER 4

EXPERIMENTAL PROCEDURES AND TECHNIQUES

4.1   COMSOL Implementation

Step 1: Specifying the problem type

In this problem, it is mass transfer by migration with no diffusion or convection. The problem dealt with electrochemistry physics.

1. COMSOL was started by double clicking on the icon
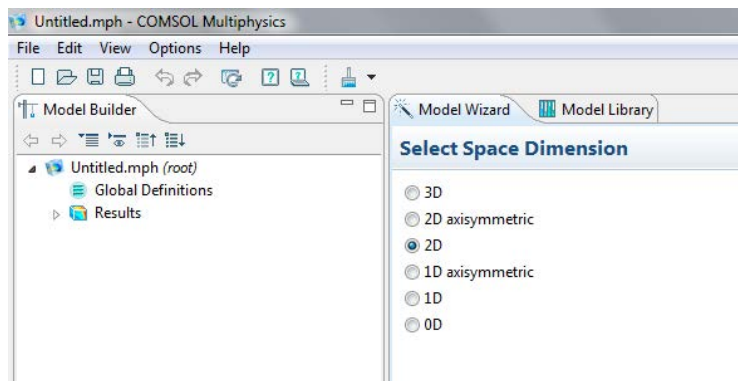
2. 2D was selected from the Select Space Dimension

FIGURE 4.1. Selection of space domain

3. Using next arrow (Blue colored arrow on the Select Space Dimension), in Add Physics, Electrochemistry >Electrodeposition, Deformed Geometry> Electrodeposition, Secondary module was selected and again using next arrow (Blue colored arrow on the Add Physics), In Study type, Time dependent study was selected.

4. Using next arrow (Blue colored arrow on the Select Study Type) Finish was selected (flag shaped icon).
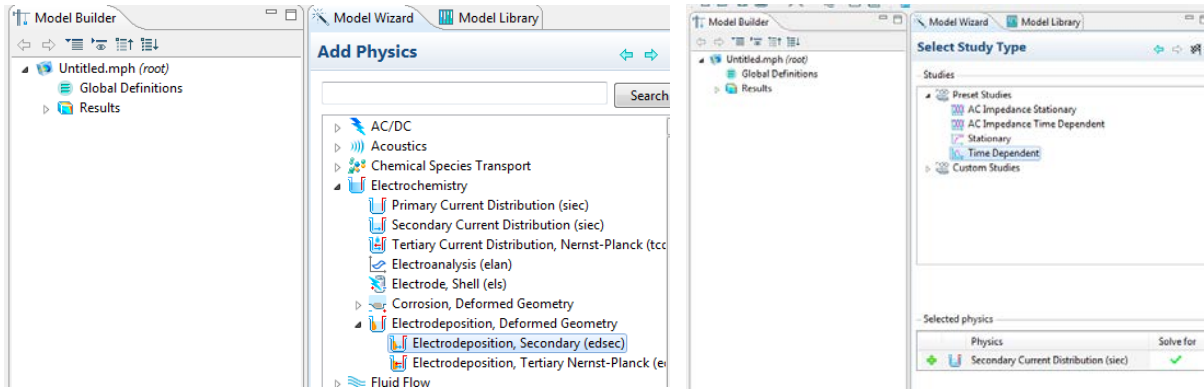
FIGURE 4.2. Selection of physics module and time study

5. The length unit was changed to cm from the default units.

6. Under the file menu, the file was saved as Cu deposition with .mph as the extension

Step 2: Setting the geometry

The geometry in this case was square.

1. Square was selected by using right click on geometry

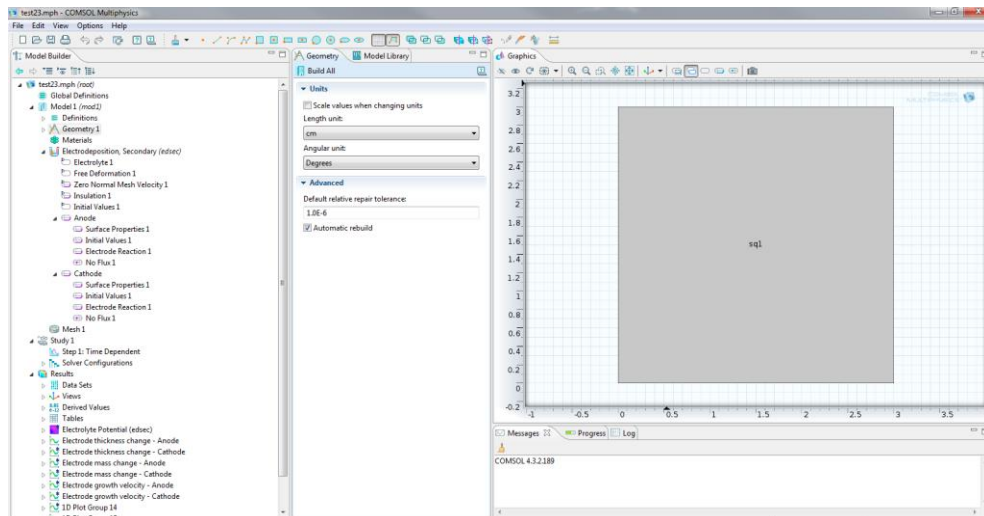2. The side length of 3 was selected and Build Selection was selected.

FIGURE 4.3. Geometry selection

Step 3: Defining electrode and electrolyte properties

1. In this step, the electrolyte, anode and cathode were defined with their properties.

36

2. Under the Electrodeposition Secondary, Electrolyte, the properties of electrolyte were entered. In the electrolyte conductivity section, User Defined was selected and the value of 4.23 [84] was entered and the other parameters were with default values.

3. External depositing electrode was created using the right click on Electrodeposition Secondary and was renamed as Anode.

4. Step 3 was repeated and it was renamed as Cathode.

5. For the Anode, Using Manual option in Selection, Boundary 3 was selected using add to selection ('+' symbol).
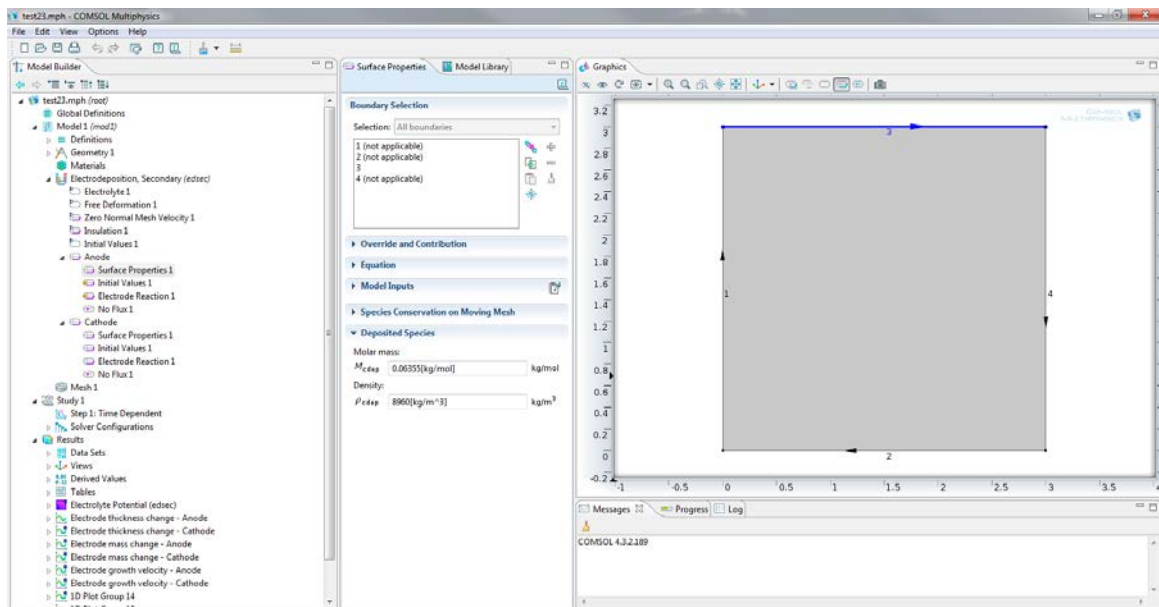

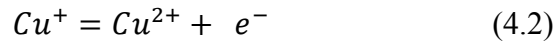FIGURE 4.4. Defining electrode properties (Anode)

6. Surface properties of the anode were defined molar mass $M_{cdep} = 0.06355 \ kg/mole$[84] (Copper Anode) and density $\rho_{cdep} = 8960 \ kg/m^3$ [84]

7. Initial values were with default values.

8. In Electrode reaction, properties were

   Model Inputs – Temperature was defined to be 293.15K

Equilibrium potential - E_{eq}, was user defined. $E_{eq,ref} = -0.34\ V$[84] (Half-cell potential)

Electrode Kinetics – Linearized Butler Volmer Kinetics expression was selected, with exchange current density $i_0 = 1e3\ A/m^2$, and anodic and cathodic coefficients as 0.5 each.

Stoichiometric coefficients – Number of participating electrons as 2, and stoichiometric coefficient to be '-1' (oxidation)

$$Cu = Cu^+ + e^- \qquad (4.1)$$

$$Cu^+ = Cu^{2+} + e^- \qquad (4.2)$$

The remaining parameters were with the default values

9. No flux parameters were with the default values.

10. For the Cathode, Using Manual option in Selection, Boundary 2 was selected using add to selection ('+' symbol).
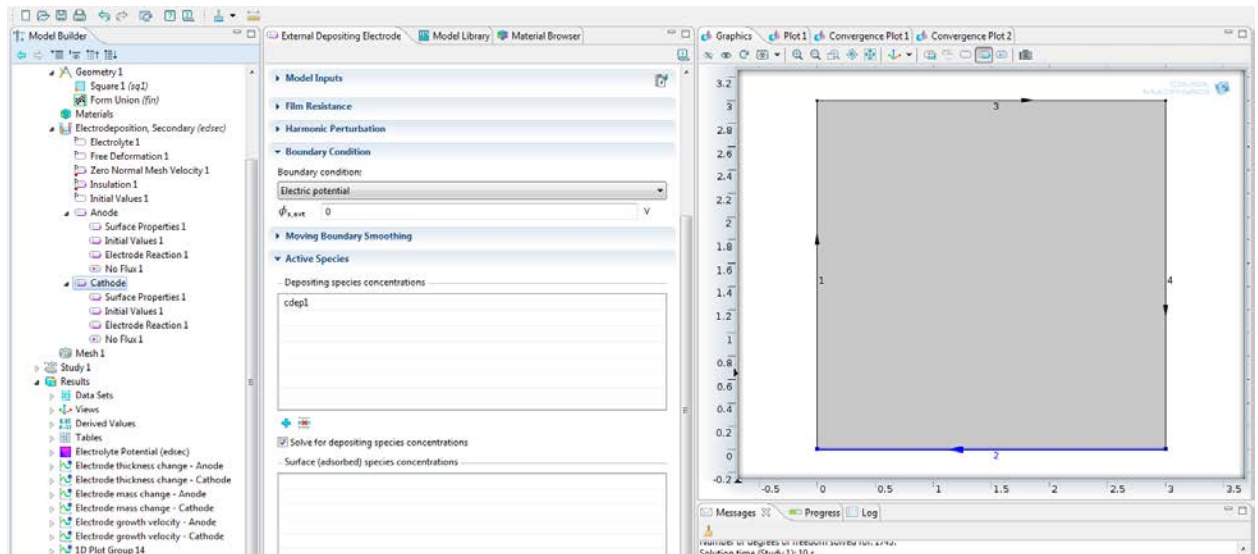

FIGURE 4.5. Defining electrode properties (Cathode)

11. Surface properties of the cathode were defined molar mass $M_{cdep} = 0.111\ kg/mole$[84] (Cobalt Chrome Cathode) and density $\rho_{cdep} = 8500\ kg/m^3$ [84]

12. Initial values were with default values.

13. In Electrode reaction, properties were

Model Inputs – Temperature was defined to be 293.15K

Equilibrium potential - E_{eq}, was user defined. $E_{eq,ref} = +0.34\ V$,[84] (Half-cell potential)

Electrode Kinetics – Linearized Butler Volmer Kinetics expression was selected, with exchange current density $i_0 = 1e3\ A/m^2$, and anodic and cathodic coefficients as 0.5 each.

Stoichiometric coefficients – Number of participating electrons as 2, and stoichiometric coefficient to be '+1' (reduction)

$$Cu^{2+} + e^- = Cu^+ \qquad\qquad (4.3)$$

$$Cu^+ + e^- = Cu \qquad\qquad (4.4)$$
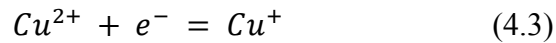
The remaining parameters were with the default values

14. No flux parameters were with the default values.

15. Between Boundary 3 and Boundary 2 is the Electrolyte.

Step 4: Meshing

In this step, the model geometry was divided into small elements

1. Physics controlled mesh was selected

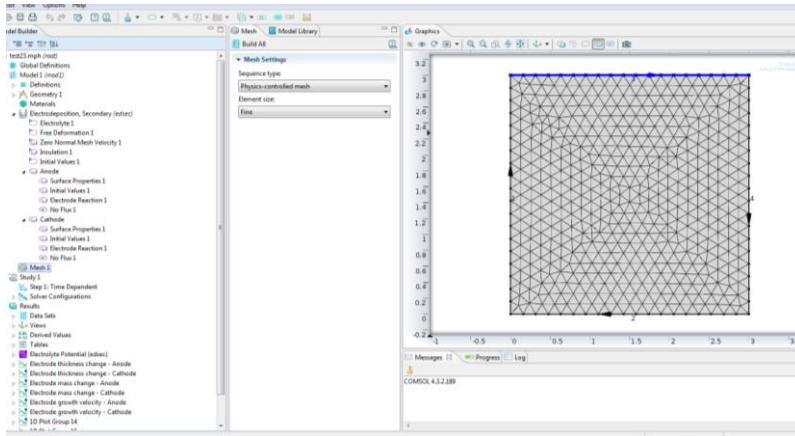2. The element size was selected to be fine

FIGURE 4.6. Defining mesh

Step 5: Defining the Study

In Step: Time Dependent

Study Settings, The time range was defined as (0, 1, 3000). This means in steps of 1sec starting from 0sec to 3000sec. And, the remaining parameters were default values.
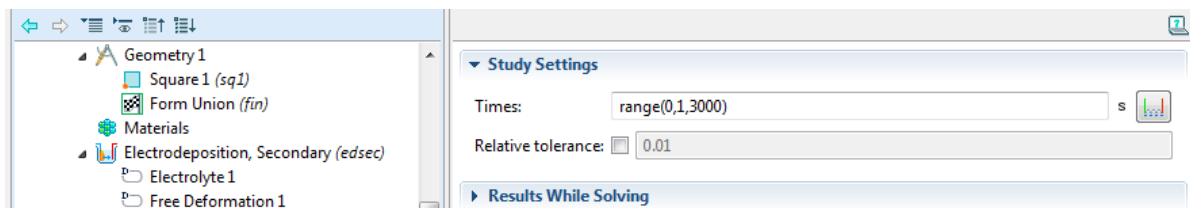

FIGURE 4.7. Study Time Settings

Step 6: Compute

The simulated was computed with right click on Compute (F8).

Step 7: Results

1. 1D plot group was created using on right click on Results.

2. Line graph was created using the right click on 1D plot group.

   Data- Solution 1 was selected from the Data set

   Time Selection – All

   Selection – Using Manual, Boundary 2(Cathode) was selected

X axis data – Time scale {Solver >Time (t)} was selected using replace

expression ( ) and check in description.

Y axis data – Thickness change was selected using the replace expression

(Electrodeposition, Secondary > Total Electrode thickness change) with unit as mm and

check in description.

It was plotted using Plot icon on the Line Graph (F8).

3. Step 2 was repeated for anode thickness change. Boundary 2 was selected at the Selection

   for this plot.

4. Step 2 was repeated for different parameters in Y for mass change and electrode growth

   velocity.

4.2 Experimental Methodology

4.2.1 Electroplating

The electroplating of Copper on Cobalt- Chrome was conducted in a electrolytic cell as shown in

the FIGURE 4.8. Solution was prepared with $100 \, gms.$ of $CuSO_4$ in $100 \, ml$ of distilled water

and $7 \, ml$ of 1N of H_2SO_4. The solution was kept on the stirrer to mix homogenously. A cobalt

chrome strip of $14cm * 14cm$ was taken and an immersion area $1.4cm * 1.4cm$ cm was used

and copper strip of $14cm * 14cm$ was taken and an immersion area $1cm * 1cm$ was used. The

copper strip was connected to the anode and the cobalt chrome was connected to the cathode

were immersed in the electrolyte and then current was passed. FIGURE 4.8 shows the image of

the experimental used for the electrodeposition process. Electroplating was conducted under the

following parameters: Conductivities: $4.23 \, S/m^2$, $1.9 \, S/m^2$, $0.93 \, S/m^2$, $0.54 \, S/m^2$ and current

density: $3.57E02 \, A/m^2$, $2.52E02 \, A/m^2$, $6.12E02 \, A/m^2$,and for different time durations. The

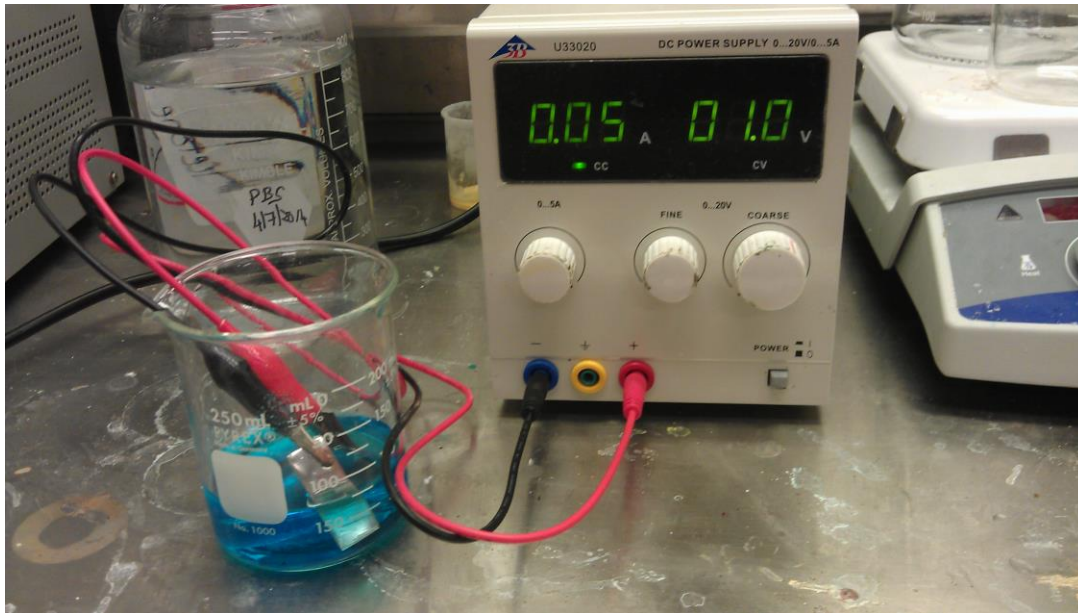samples were then characterized with microscope, SEM EDS and thickness gage.

FIGURE 4.8 Experimental Setup of the electrodeposition process

4.2.2 Effect of Current Density

Current density[85] is the electric current per unit area of cross section and measured in amperes

per square metre. Solution with conductivity of $4.23\ S/m^2$

($18.8\ g\ of\ CuSO_4\ in\ 100ml\ of\ distilled\ water\ and\ 7ml\ of\ 1N\ H_2SO_4$) was used and

thickness was calculated using different current densities - $2.52E02\ A/m^2$

($0.05A\ over\ area\ of\ 1.4cm * 1.4cm$), $3.57E02\ A/m^2$ ($0.07A\ over\ area\ of\ 1.4cm * 1.4cm$)

and $6.12E02\ A/m^2$ ($0.12A\ over\ area\ of\ 1.4cm * 1.4cm$) for a duration of $18\ min$, $25\ min$,

$40\ min$ and $46\ min$ respectively.

4.2.3 Effect of electrical conductivity of the electrolyte

The electrical conductivity [86] of an electrolyte solution is the ability to conduct electricity. The

unit of conductivity is siemens per meter (S/m). Test parameters used were: conductivity:

$4.23\ S/m^2$ ($18.8\ g\ of\ CuSO_4\ in\ 100ml\ of\ distilled\ water\ and\ 7ml\ of\ 1N\ H_2SO_4$), $1.9\ S/$

m^2 (5.5 g of $CuSO_4$ in $100ml$ of $distilled$ $water$ and $7ml$ of $1N$ H_2SO_4), 0.93 S/m^2

(2.2g of $CuSO_4$ in $100ml$ of $distilled$ $water$ and $7ml$ of $1N$ H_2SO_4)   and 0.54 S/m^2

(1.2g of $CuSO_4$ in $100ml$ of $distilled$ $water$ and $7ml$ of $1N$ H_2SO_4)with   current   density

$3.57E02$ A/m^2 $(0.07A$ $over$ $area$ of $1.4cm * 1.4cm)$ and for a $35 - 40$ min duration.

4.3 Characterization

4.3.1   Optical Microscopy

The computer was integrated with The Leica Optical Microscope (OM) and connected to a camera, which helps in studying the topography of the coated surface. The software Leica Vision was used to collect the images from the camera and performed analysis on the images. The settings of the microscope helped in the obtaining the images at different magnifications (10X, 20X), as per the experimental requirements.

FIGURE 4.9 Optical Microscope setup

4.3.2   SEM EDS

The coated sample is placed inside a vacuum tube present in the scanning electron microscope (SEM). The electrons inside the tube were generated from the heated filament which was produced using a high voltage and were focused on the sample. The sample surface

43

is conducted using a metal coating. Using electron beams, SEM generates an image of the coating sample. Advantage of SEM over optical microscope is that higher magnification of the sample can be obtained. Limitation of the SEM, it cannot image any irregular topographical features.

The x-rays generated by the electrons reflected by the sample could be analyzed using energy dispersive spectroscopy (EDS) to understand the composition of the atoms on the sample. Few elements that are heavier than Boron cannot be detected by this process. The sample size used for the analysis is couple of cubic centimeters.

FIGURE .4.10 SEM apparatus

4.3.3 Thickness Measurement

Coating thickness gauge

Coating thickness gauge of the series DCFN 3000EZ was used in the experiment. The gauge consists of a LCD display, zero key, statistics key, ON/OFF switch and battery compartment (on the rear).The DCFN -3000EZ will mechanically identify whether the testing material is ferrous or non-ferrous metal and will show the accurate reading on the display.

It offers quick, non-destructive and accurate coating measurements on ferrous and non-ferrous metals. The gauge is used for various laboratory applications and also for testing the non-

magnetic coatings on steel and ferrous metals and electrically insulating coatings on non-ferrous metals. The measurements in the ferrous mode are conducted using the magnetic induction method and in the non-ferrous mode through the Eddy current method. Using the factory calibration we can measure the flat and slightly curved surfaces and Zero procedure is used to measure the curved and rough surfaces.

FIGURE 4.11 Coating thickness gauge

SEM EDS

SEM EDS was used to analyze the coating thickness of the sample. Coated samples were dipped in liquid nitrogen, and the coated layer was peeled and used for analysis. The sample was placed in the SEM and electron beam reflected was to study the elemental composition and the thickness of the coated layer. Detailed explanation of the procedure was given in Sec 4.3.2.

CHAPTER 5

RESULTS AND DISCUSSION

5.1 Simulation of electrodeposition

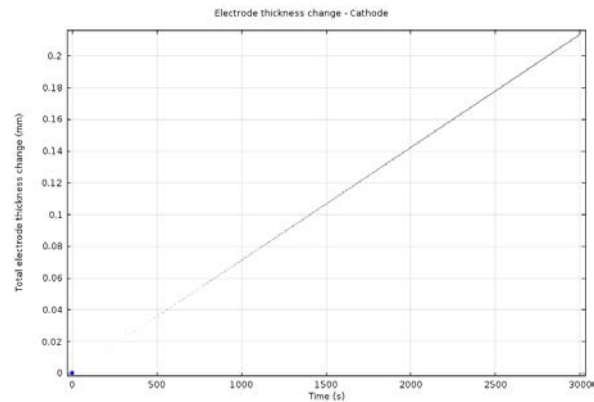## 5.1.1 Thickness change over time

FIGURE 5.1 .Copper coating thickness change of cathode as a function of time

Thickness change over time was plotted as a function of time for cathode in the FIGURE 5.1. Along the Y axis was the thickness change. The simulation predicted, for the first 500 sec the coating was not started, after that there was a steady coating of Cu on Co-Cr. At the end of 3000 sec, coating was at 0.22mm layer on the Co- Cr.
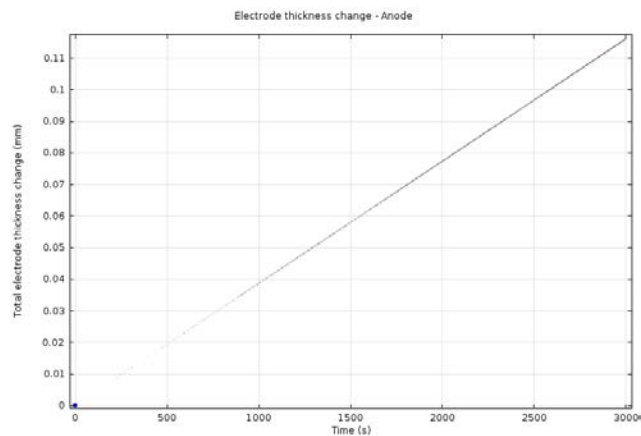

FIGURE 5.2. Copper coating thickness change of anode as a function of time

Thickness change over time was plotted as a function of time for anode in the FIGURE 5.2. Along the Y axis was the thickness change. The simulation predicted that for the first 500 sec the thickness change of anode was not steady. After that, the degradation of the Cu was slow at the initial time periods, later it started increasing. The layer degraded by about 0.15mm.
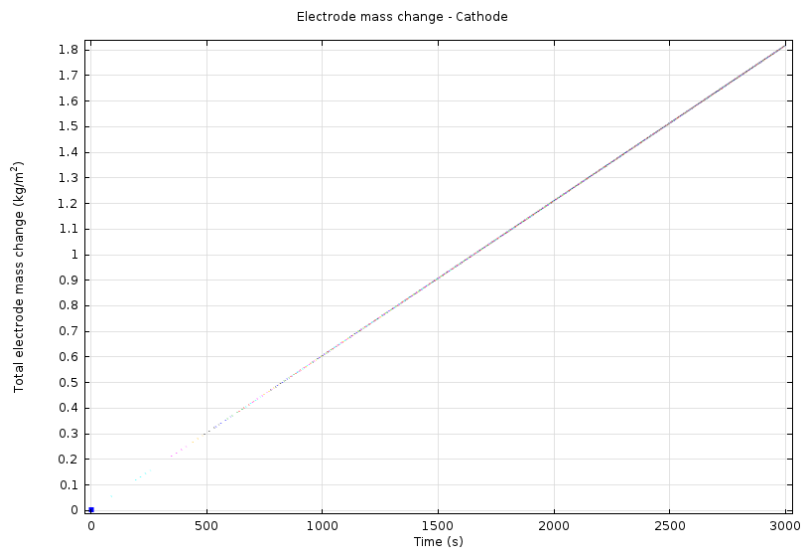
5.1.2 Mass change over time

FIGURE 5.3. Mass change of cathode as function of time

Mass change of cathode over time plotted as a function of time in the FIGURE 5.3. Along the Y axis was the cathode electrode mass change. Simulation predicted the mass change of the cathode at the end of 3000 sec to be 1.8 kg/m^2. Meaning, the mass deposition on the cathode was 1.8 kg/m^2. The total copper deposited on the cobalt chrome could be accounted for this mass increment.
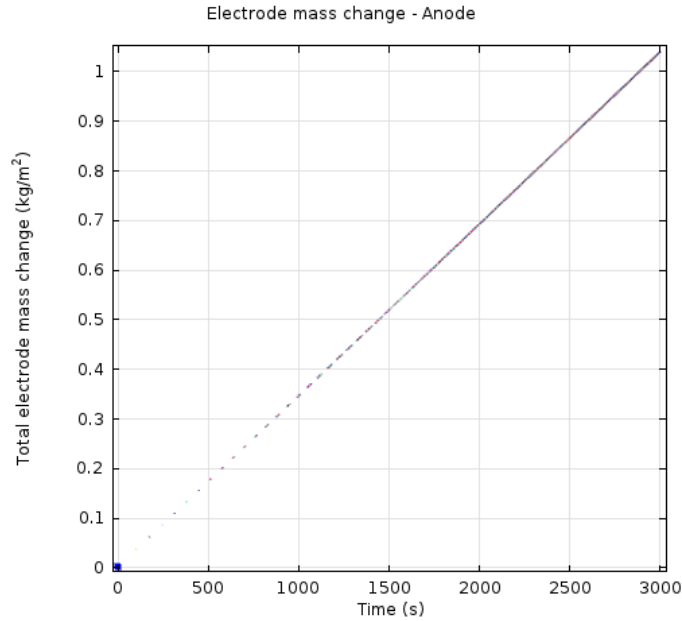
FIGURE 5.4. Mass change of anode as function of time

Mass change of anode over time plotted as a function of time in the FIGURE 5.4. Along the Y axis was the anode electrode mass change. Simulation predicted the mass change of the anode at the end of 3000 sec was 1.2 kg/m^2. Meaning, the mass deposition on the cathode was 1.2 kg/m^2. The copper lost on the copper electrode could be accounted for this change in the mass loss.

5.1.3 Fraction of free sites over spatial coordinate
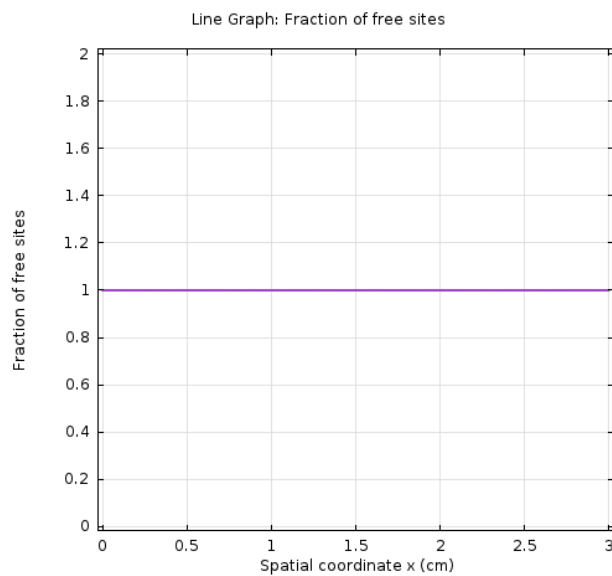

FIGURE 5.5. Fraction of free sites as function of spatial coordinate

In FIGURE 5.5, fraction of sites as function of spatial coordinate was plotted. Fraction of free sites indicated the conversion ratio of the final product from the initial reactants. Simulated predicted "1", explaining the solid was completely formed from the reactions on the cathode.

5.2 Electrodeposition of Copper on Cobalt Chrome

5.2.1 Copper coating thickness at thirty minutes

This test was conducted to check the variability of the results of the experiment with same parameters. Test parameters were, conductivity - $4.23\ S/m^2$, current density $-\ 3.57\ +\ E2\ A/m^2$ and for 30 min duration on a $1.4\ cm * 1.4\ cm$ area of contact. The test was conducted on four samples with same experimental setup and conditions. The results from the experiment were tabulated with the standard error (SE) (TABLE 5.1) and thickness was measured using the SEM and thickness gauge. For the SEM, the sample was dipped in liquid nitrogen for few minutes. Once the sample was cold enough, it was hammered to separate the coated layer. This layer was used to measure the thickness. Thickness gauge was directly used on the sample to measure the thickness. For each sample measurements were taken at different points and then averaged.

TABLE 5.1

THICKNESS DATA OF THE FOUR SAMPLES USING SEM AND THICKNESS GAUGE

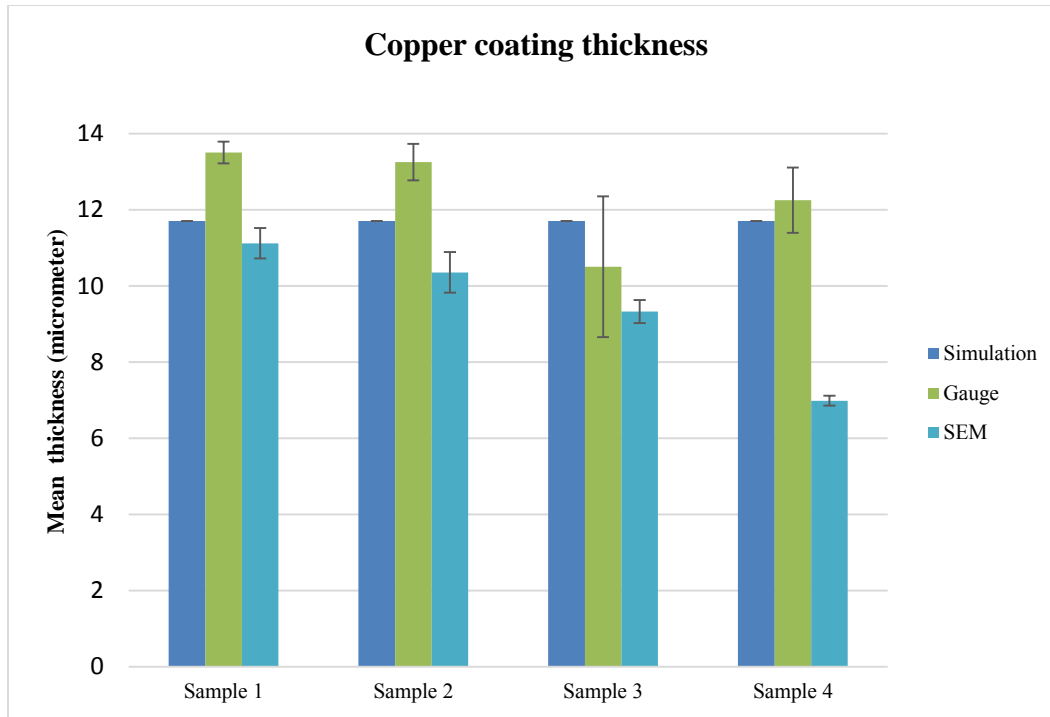|	Current	Duration	Thickness (micrometer)		
			Simulation	SEM (Mean +/-SE)	Gauge (Mean +/-SE)
Sample 1	0.07 A	30 min	11.7	11.12+/-0.4	13.5+/-0.29
Sample 2	0.07 A	30 min	11.7	10.35+/-0.53	13.25+/-0.48
Sample 3	0.07 A	30 min	11.7	9.33+/-0.3	10.5+/-1.85
Sample 4	0.07 A	30 min	11.7	6.98+/-0.13	12.25+/-0.85

FIGURE 5.6 Graph showing the thickness using simulation, gauge and SEM values at 30

minutes

The above graph (FIGURE 5.6) shows the thickness of the coating using all the three experiments: Simulation, SEM and Thickness Gauge. It was observed that there was lot of variation in SEM over the gauge. This variation could be attributed to the plane in which thickness values were recorded. Each sample's coating layer was not a clean peel for the exact thickness measurement. The layer was not uniform when it was removed from the cathode and the plane was not 100% planar when it was measured. This caused the change in the thickness values for the different samples. Thickness gauge was very sensitive to the pressure applied while measuring the sample. Small variation in the pressure showed different values.
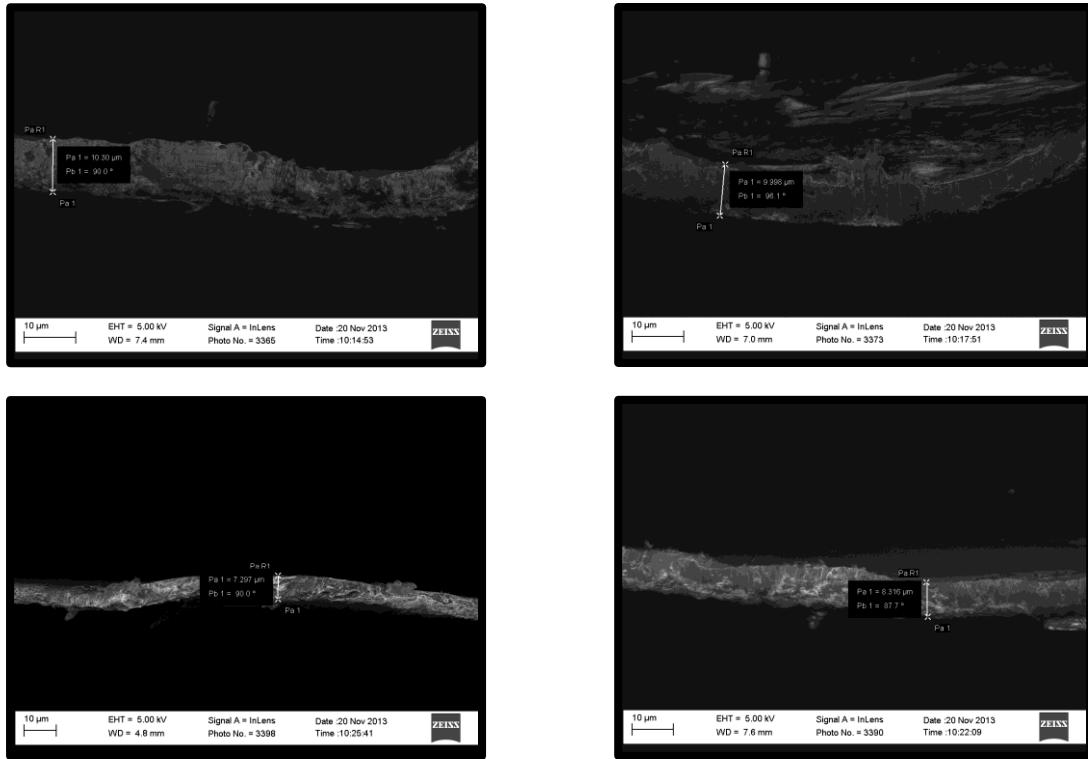
FIGURE 5.7 SEM Images of the four samples at 0.07 A for a duration of 30 min

5.2.2 Effect of current density on coating thickness

This experiment was conducted with different current densities at a conductivity of $4.23\ S/m^2$ on $1.4\ cm * 1.4\ cm$ area of contact. The values of the experiment are tabulated (TABLE 5.2) along with the simulation result values under same conditions. The different current densities used were $2.50\ E + 02\ (A/m^2)$, $3.57\ E + 02\ (A/m^2)$ and $6.12\ E + 02\ (A/m^2)$. By increasing or decreasing the current density the flow of electrons were affected. Increasing current density, the flow of electrons in the electrolyte increased causing the coating layer to increase in thickness (TABLE 5.2).

51

TABLE 5.2

THICKNESS DATA OF THE SAMPLES WITH DIFFERENT CURRENT DENSITIES

Thickness (micrometer)			
Current Density - 2.50 E+02 (A/m^2)			
Time (min)	Simulation	SEM (Mean +/-SE)	Gauge (Mean +/-SE)
18	7	2.33+/-0.09	5+/-0.41
25	9.5	4.65+/-0.31	6.75+/-0.48
40	14.3	6.9416+/-0.09	11.5+/-1.19
46	17.3	7.3912+/-0.23	10.2+/-0.73
Current Density - 3.57 E+02 (A/m^2)			
Time (min)	Simulation	SEM (Mean +/-SE)	Gauge (Mean +/-SE)
18	7	1.8275+/-0.13	6.25+/-0.48
25	9.6	9.987+/-0.62	6+/-0.41
40	15	1.5996+/-0.09	10.4+/-0.1.03
46	17.6	13.455+/-0.47	11.8+/-0.37
Current Density - 6.12 E+02 (A/m^2)			
Time (min)	Simulation	SEM (Mean +/-SE)	Gauge (Mean +/-SE)
18	7	8.68+/-0.9	4.4+/-0.81
25	9.8	8.964+/-0.34	8+/-0.45
40	15.2	23.49+/-1.27	34+/-1.87
46	18	31.35+/-2.43	42.75+/-1.25

The graph was plotted with different current densities for duration of 46 minutes.
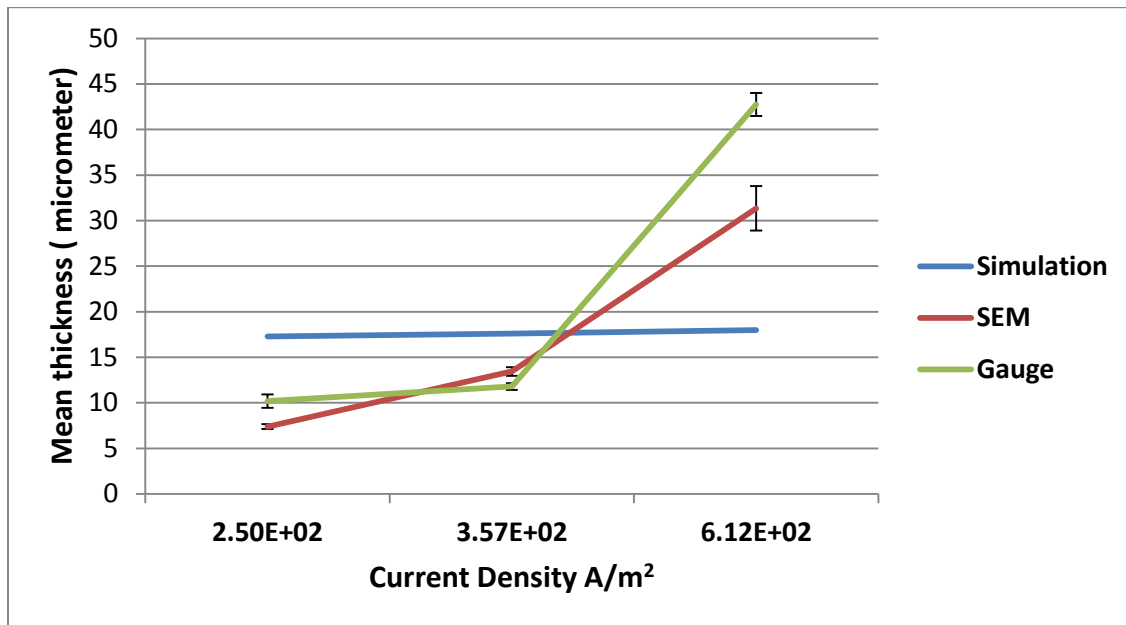

FIGURE 5.8 Graph showing thickness with different current densities at duration of 46 minutes

The above graph (FIGURE 5.8) shows an increase in trend with increase in current density with all the three experiments. SEM showed nearly the same thickness as gauge at 46 minutes. The variation for different values (for example at $6.12\,E02\,A/m^2$, simulation $-$ 18 µm, SEM $-$ 31.35 µm, gage $-$ 42.75 µm) from the simulation results could be due to the measurement error and limitations in SEM and gauge. Possible explanation for this could be the layer resistance caused by the coating from the previous coated layer. Simulation doesn't account for this resistance caused in the coating.

Coating thickness at current density $6.12\,E02\,A/m^2$

In the FIGURE 5.9, the thickness was plotted vs current density of $6.12\,E02\,A/m^2$. There was an increasing trend observed in the thickness over the time. All three experiments

showed the increasing trend over the time. The deviation (simulation – 18 μm, SEM – 31.35 μm, gage – 42.75 μm) could be accounted for the SEM and gauge limitations.

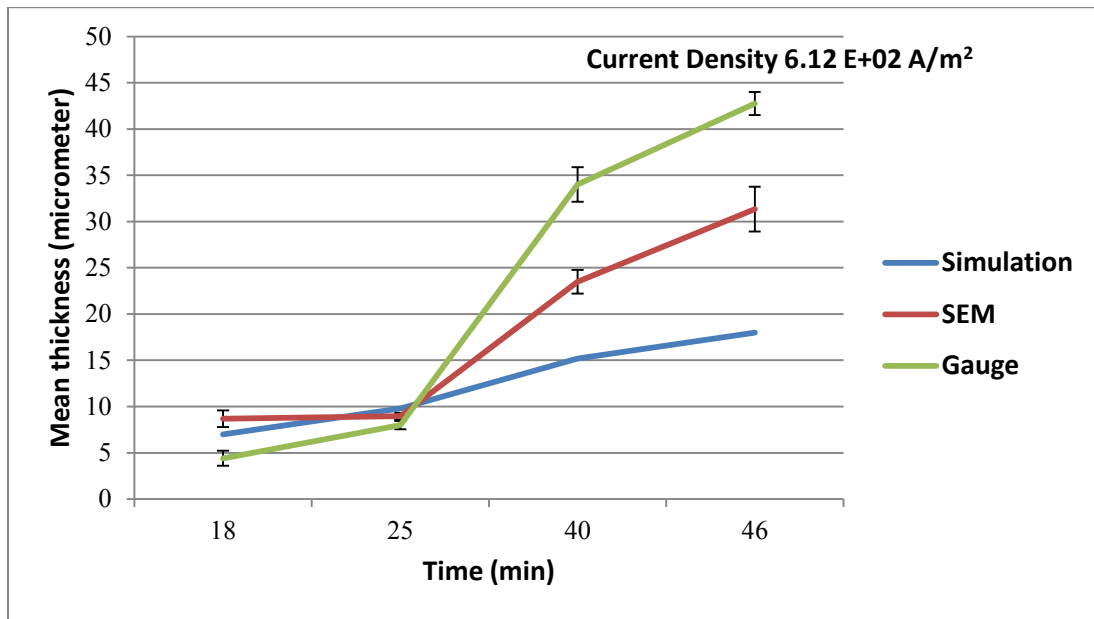
FIGURE 5.9 Graph showing thickness vs. time at $6.12E + 02\ A/m^2$ with simulation, SEM and gauge
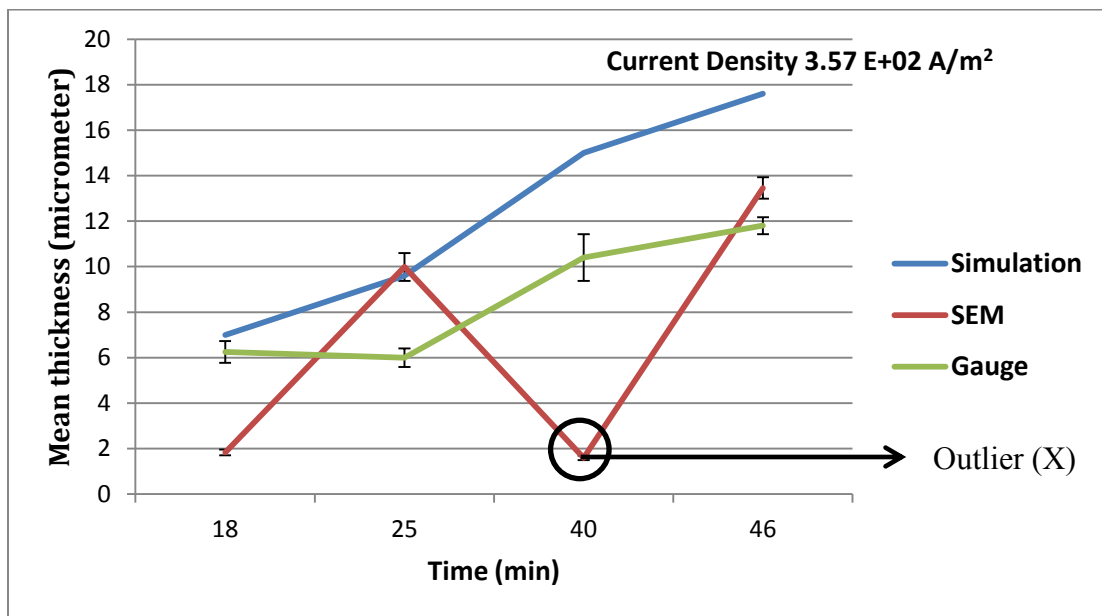
Coating thickness at current density 3.57 E02 A/m^2

FIGURE 5.10 Graph showing thickness vs. time at $3.57E + 02\ A/m^2$ with simulation, SEM and

gauge

In the FIGURE 5.10 there was an increasing trend line with increase in duration. Both simulation and gauge showed the increasing trend. Only SEM at 40 minute had a dip in the trend. This could be an outlier. Deviation from the simulation could be the limitations of SEM and gauge measuring techniques. Experiment was repeated to check the outlier data point. It was conducted and it was verified to be a good coating with good finish (FIGURE 5.11). The data point(X) in the experiment was confirmed to be an outlier.

FIGURE 5.11 Coating at 3.75E2 A/m$_2$ for 30 minutes at 4.23 S/m^2

Coating thickness at current density 2.5 E02 A/m^2

In the FIGURE 5.12, there was an increasing trend in the graph. All the three experiments showed an increasing trend in the thickness over the time. The dip at the 46-minute in gauge was caused due to measurement limitation. The sample had big standard error, which could be due to the measuring technique.
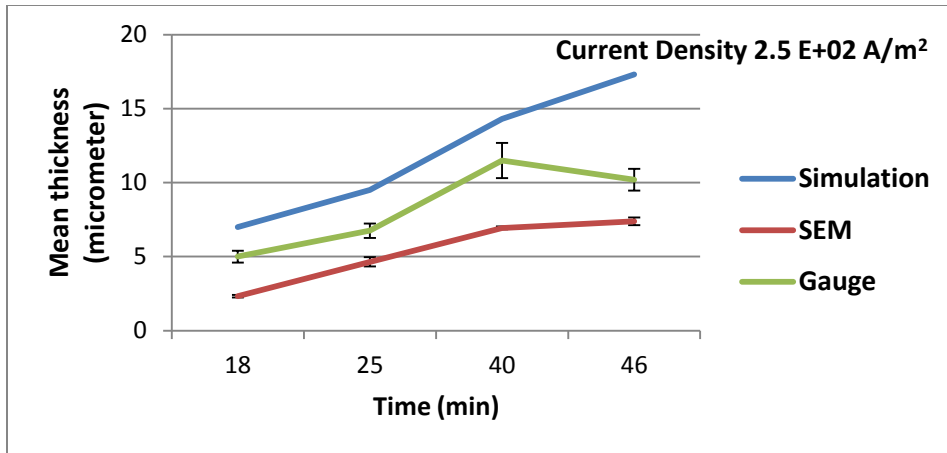
FIGURE 5.12 Graph showing thickness vs. time at 2.5E+02 A/m^2 with simulation, SEM and

gauge

A   B
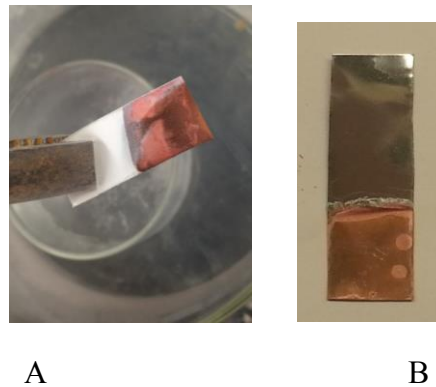
FIGURE 5.13 Thickness variations with different current densities
A. Coating at low current densities ($2.5 + 02\ A/m^2$), B. Coating at high current densities
($6.12E + 02\ A/m^2$)

FIGURE 5.13 shows the images of the electrodeposition at different current densities

FIGURE 5.14 shows the tabulated SEM images of the electrodeposition at different current

densities for different durations

	18 min	25 min	40 min
0.05 A			
0.07A			
0.12 A			
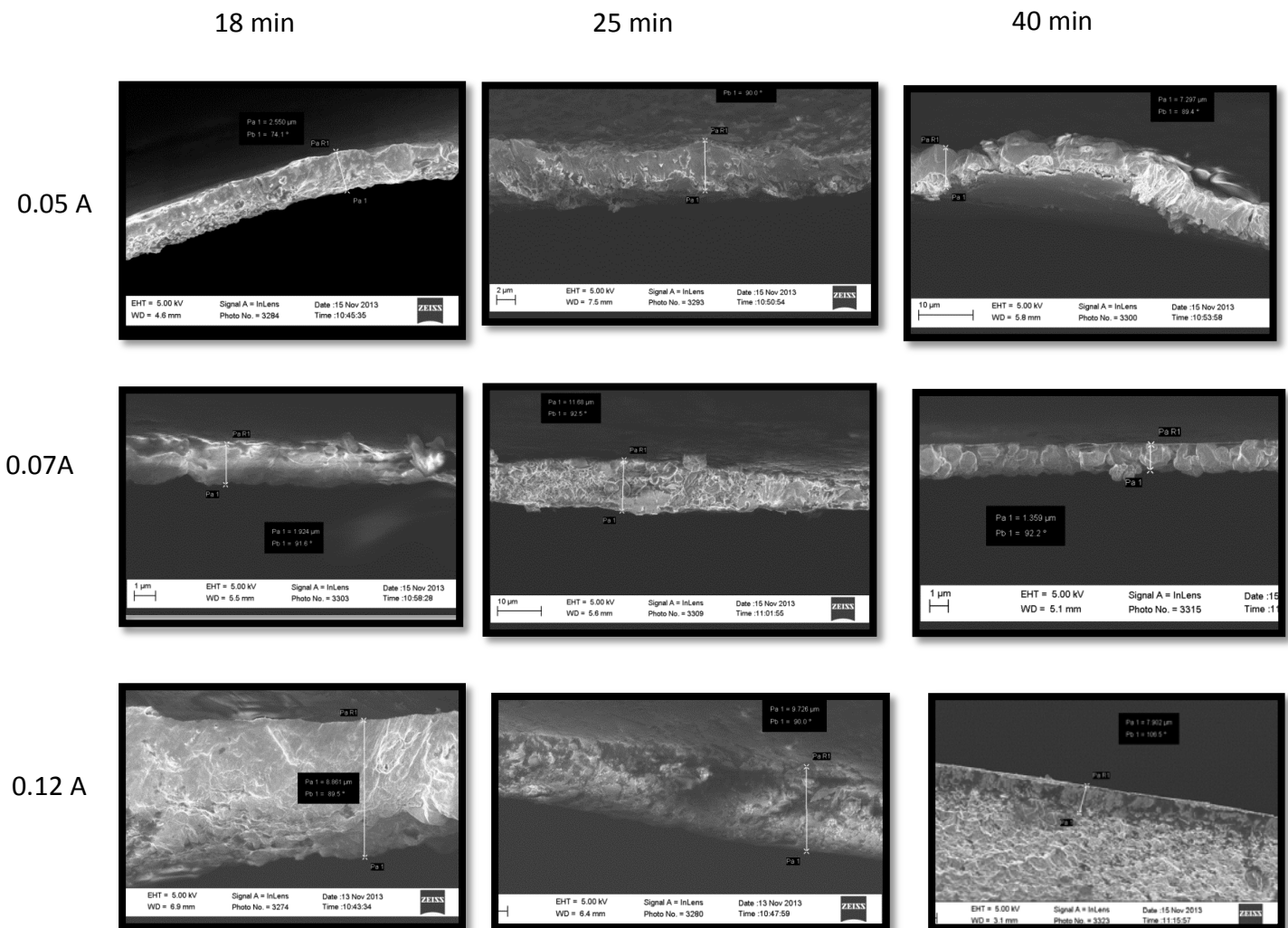
FIGURE 5.14 SEM images of the copper coated

5.2.3 Effect of conductivity on coating thickness

This test was conducted with different electrical conductivities of the electrolyte keeping the other parameters constant (duration $35 - 40\ min$, current density $3.57 + E2\ A/m^2$). Test parameters were, conductivity - $4.23\ S/m^2$, $1.9\ S/m^2$, $0.93\ S/m^2$ and $0.54\ S/m^2$ on a $1.4\ cm *$ $1.4\ cm$ area of contact. The results from the experiment are tabulated (TABLE 5.3) and thickness was measured using the SEM and thickness gauge.

TABLE 5.3

THICKNESS DATA OF THE SAMPLES WITH DIFFERENT CONDUCTIVITIES

	Thickness (micrometer)			
Conductivity (E02 S/m^2)	4.23	1.9	0.93	0.54
Simulation	15	6	2	1.6
Gauge	10.4	2	0	0
SEM	1.6	0	0	0
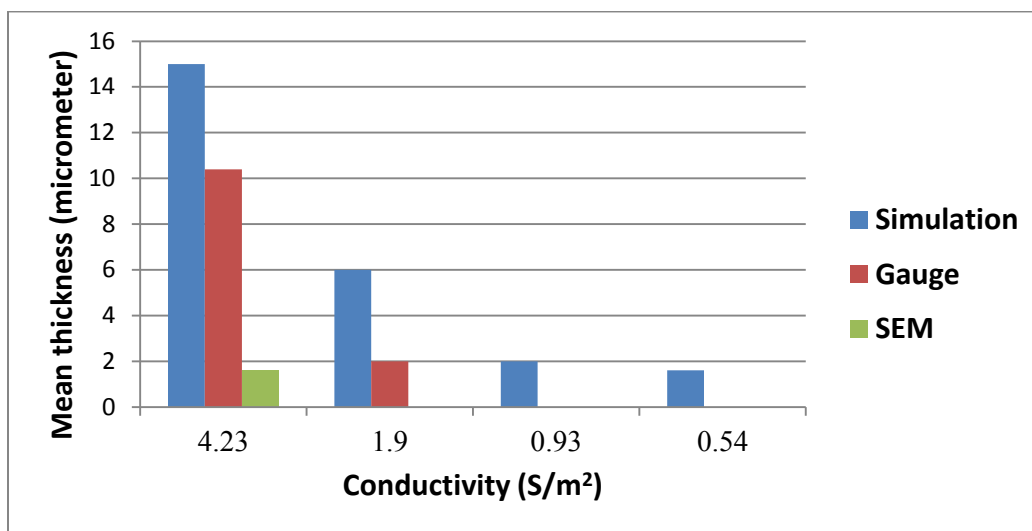
FIGURE 5.15 Coating thicknesses with different conductivities with simulation, gauge and SEM

In the FIGURE 5.15, decreasing trend in the thickness coating was observed with decrease in the electrical conductivity of the electrolyte. The experiment was conducted for duration of $35 - 40$

minutes. As the conductivity lowered ($0.93\ S/m^2$ and $0.54\ S/m^2$) the coating was not even and was powdery (FIGURE 5.17). All the three experiments showed a decreasing trend in the thickness deposition. At 1.9 S/m², 0.93 S/m² and 0.54 S/m² SEM was not performed as the coating was powdery. EDS was performed to confirm the powdery substance (FIGURE 5.16). It was verified to be copper. The electrolyte conductivity was not sufficient for a good coating onto the metal surface. With decrease in the conductivity levels the coating became thinner, non-uniform and weak.

FIGURE 5.16 EDS graph showing the presence of copper in the powder sample

FIGURE 5.17 Powdery coating at low conductivity

CHAPTER 6

SUMMARY AND RESULTS

The simulation was conducted and experimental validation of electrodeposition was performed. The results had a trend justifying the simulation output with the experiment values. The rea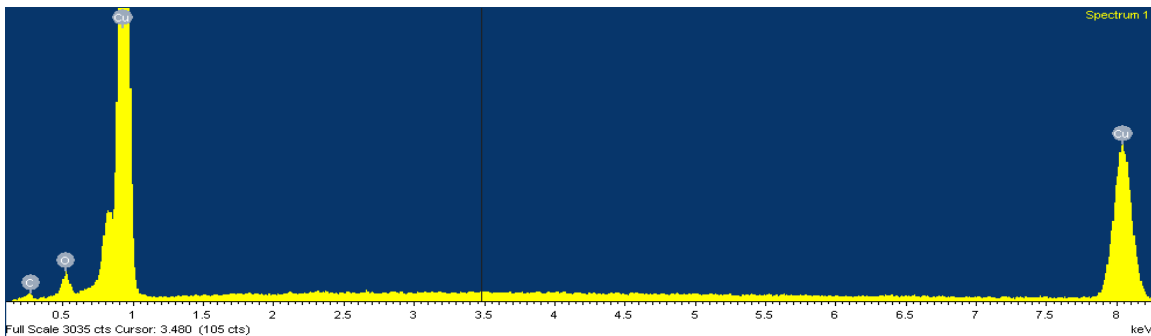son for the deviation of the results was because of some limitations. The pre-activation procedure difference was not accounted by the simulation model. The pre-activation helps to activate the surface of the metal helping in better coating during when the experiment is being performed. Layer over layer coating has influence over the next coating layer, which the simulation doesn't account for the thickness calculation. Practically, there is a limitation for the electrical conductivity constant based on the concentration levels, which the simulation doesn't account in the model. It accepts any value for conductivity, which is practically not true. The procedure for the SEM measurement had limitations. The way in which the coating was peeled from the sample using nitrogen liquid was not a perfect and clean peel. Any small bent on the edge line of the layer, had a big impact on the measurement using the SEM. These were very sensitive which were difficult to control during the peeling procedure. The plane of the measurement angle also played a role in the variation of the thickness. The coated layer wasn't planar, small variation in angle showed lot of difference in the values. The thickness gauge was very sensitive to the pressure applied on the surface. Small variations in the pressure showed a big difference in the output. These were the limitations that caused the variability in the results.

FUTURE WORK

For the future work, the variability and limitations faced during the model development and the experimental procedures need to be addressed. A standard protocol has to be developed

for the measurement process for both SEM and thickness gauge. More experiments are to be conducted using different substances with different electrolyte to understand the limitations of the simulation software.

REFERENCES

REFERENCES

[1] Rahman MA, Pakštas A, Wang FZ. Network modelling and simulation tools. Simulation Modelling Practice and Theory. 2009;17:1011-31.

[2] Levytskyy A, Vangheluwe H, Rothkrantz LJM, Koppelaar H. MDE and customization of modeling and simulation web applications. Simulation Modelling Practice and Theory. 2009;17:408-29.

[3] Haronian D. Maximizing microelectromechanical sensor and actuator sensitivity by optimizing geometry. Sensors and Actuators A: Physical. 1995;50:223-36.

[4] Devarakonda M, Brooks K, Rönnebro E, Rassat S. Systems modeling, simulation and material operating requirements for chemical hydride based hydrogen storage. International Journal of Hydrogen Energy. 2012;37:2779-93.

[5] Wilson PF, Ma MT, Adams JW. Techniques for measuring the electromagnetic shielding effectiveness of materials. I. Far-field source simulation. Electromagnetic Compatibility, IEEE Transactions on. 1988;30:239-50.

[6] Nakajo A, Wuillemin Z, Van herle J, Favrat D. Simulation of thermal stresses in anode-supported solid oxide fuel cell stacks. Part I: Probability of failure of the cells. Journal of Power Sources. 2009;193:203-15.

[7] Hettelingh JP, Gardner RH, Hordijk L. A statistical approach to the regional use of critical loads. Environmental Pollution. 1992;77:177-83.

[8] Darmont J, Attoui A, Gourgand M. Simulation of clustering algorithms in OODBs in order to evaluate their performance. Simulation Practice and Theory. 1997;5:269-87.

[9] Illy BN, Cruickshank AC, Schumann S, Da Campo R, Jones TS, Heutz S, et al. Electrodeposition of ZnO layers for photovoltaic applications: controlling film thickness and orientation. Journal of Materials Chemistry. 2011;21:12949-57.

[10] Lihua L, Xiuqin Z, Xianfeng L, Haowei W, Naiheng M. Effect of silicon on damping capacities of pure magnesium and magnesium alloys. Materials Letters. 2007;61:231-4.

[11] Shadanbaz S, Dias GJ. Calcium phosphate coatings on magnesium alloys for biomedical applications: A review. Acta Biomaterialia. 2012;8:20-30.

[12] Wan P, Lin X, Tan L, Li L, Li W, Yang K. Influence of albumin and inorganic ions on electrochemical corrosion behavior of plasma electrolytic oxidation coated magnesium for surgical implants. Applied Surface Science. 2013;282:186-94.

[13] Huang W, Wang M, Wang H, Ma N, Li X. The electrodeposition of aluminum on TiB2/A356 composite from ionic liquid as protective coating. Surface and Coatings Technology. 2012;213:264-70.

[14] Moral-Vico J, Carretero NM, Pérez E, Suñol C, Lichtenstein M, Casañ-Pastor N. Dynamic electrodeposition of aminoacid-polypyrrole on aminoacid-PEDOT substrates: Conducting polymer bilayers as electrodes in neural systems. Electrochimica Acta. 2013;111:250-60.

[15] O'Mullane AP. Electrochemistry. Reference Module in Chemistry, Molecular Sciences and Chemical Engineering: Elsevier; 2013.

[16] Song S, Shen WD, Liu MH, Song GL. Corrosion study of new surface treatment/coating for AZ31B magnesium alloy. Surface Engineering. 2012;28:486-90.

[17] Adoberg E, Podgurski V, Peetsalu P, Lind L, Mikli V, Hvizdos P, et al. The effect of surface pre-treatment and coating post-treatment to the properties of TiN coatings. Pinna eel- ja pinde järeltöötluse mõju TiN-pinde omadustele. 2012;18:185-92.

[18] Sağlam I, Özyürek D, Çetinkaya K. Effect of ageing treatment on wear properties and electrical conductivity of Cu-Cr-Zr alloy. Bulletin of Materials Science. 2011;34:1465-70.

[19] Yousfi S, Hadjoudja B, Chouial B, Djedid N, Chibani A. Heat treatment effect on the resistivity of polycrystalline silicon films. Surface Engineering. 2012;28:715-7.

[20] Wongprot T, Matan N, Matan N, Preechatiwong W, Kyokong B. Response Surface Modeling of Hydrothermal Treatment Conditions on Color Changes, Strength, and Durability Properties of Rubberwood. BioResources. 2013;8:302-12.

[21] Shenoy SP. Heat treating cost reductions due to Protective Coatings. Forging. 2012;22:18-22.

[22] Grubbs CA. Anodizing of aluminum. Metal Finishing. 2012;110:465-78.

[23] Pires I, Quintino L, Miranda RM. Performance Of 2024-T3 Aluminium Adhesive Bonded Joints. Materials & Manufacturing Processes. 2005;20:175-85.

[24] Lee H-J, Jeon H, Lee W-S. Ultrathin ultrananocrystalline diamond film synthesis by direct current plasma-assisted chemical vapor deposition. Journal of Applied Physics. 2011;110:084305.

[25] Wu J, Jiang Y, Johnson C, Liu X. DC electrodeposition of Mn–Co alloys on stainless steels for SOFC interconnect application. Journal of Power Sources. 2008;177:376-85.

[26] Podlaha EJ. Selective Electrodeposition of Nanoparticulates into Metal Matrices. Nano Letters. 2001;1:413-6.

[27] Xu J, Huang X, Xie G, Fang Y, Liu D. Fabrication and magnetic property of monocrystalline cobalt nanowire array by direct current electrodeposition. Materials Letters. 2005;59:981-4.

[28] Lee J, Chung W, Jung U, Kim Y. Direct nickel electrodeposition on magnesium alloy in pyrophosphate electrolyte. Surface and Coatings Technology. 2011;205:4018-23.

[29] Santos A, Vojkuvka L, Pallarés J, Ferré-Borrull J, Marsal LF. Cobalt and Nickel Nanopillars on Aluminium Substrates by Direct Current Electrodeposition Process. Nanoscale Res Lett. 2009;4:1021-8.

[30] Shen C-m, Zhang X-g, Li H-l. DC electrochemical deposition of CdSe nanorods array using porous anodic aluminum oxide template. Materials Science and Engineering: A. 2001;303:19-23.

[31] Chandrasekar MS, Pushpavanam M. Pulse and pulse reverse plating—Conceptual, advantages and applications. Electrochimica Acta. 2008;53:3313-22.

[32] Ett G, Pessine EJ. Pulse current plating of TiB2 in molten fluoride. Electrochimica Acta. 1999;44:2859-70.

[33] Choi Y, Kim M, Kwon SC. Characterization of chrome layer formed by pulse plating. Surface and Coatings Technology. 2003;169–170:81-4.

[34] Bradley PE, Landolt D. Pulse-plating of copper–cobalt alloys. Electrochimica Acta. 1999;45:1077-87.

[35] Wu J, Johnson CD, Jiang Y, Gemmen RS, Liu X. Pulse plating of Mn–Co alloys for SOFC interconnect applications. Electrochimica Acta. 2008;54:793-800.

[36] Emekli U, West AC. Effect of additives and pulse plating on copper nucleation onto Ru. Electrochimica Acta. 2009;54:1177-83.

[37] Datta M, Landolt D. Experimental investigation of mass transport in pulse plating. Surface Technology. 1985;25:97-110.

[38] Tang PT. Pulse reversal plating of nickel and nickel alloys for microgalvanics. Electrochimica Acta. 2001;47:61-6.

[39] Pipino ACR, Schatz GC, Van Duyne RP. A rigorous electrodynamic model for periodic structure formation during UV laser-induced metal atom deposition. Chemical Physics Letters. 1995;237:137-44.

[40] Rombouts M, Maes G, Hendrix W, Delarbre E, Motmans F. Surface Finish after Laser Metal Deposition. Physics Procedia. 2013;41:803-7.

[41] Heralić A, Christiansson A-K, Lennartson B. Height control of laser metal-wire deposition based on iterative learning control and 3D scanning. Optics and Lasers in Engineering. 2012;50:1230-41.

[42] Lou HH, Huang YL. Hierarchical decision making for proactive quality control: system development for defect reduction in automotive coating operations. Engineering Applications of Artificial Intelligence. 2003;16:237-50.

[43] Mette A, Schetter C, Wissen D, Lust S, Glunz SW, Willeke G. Increasing the Efficiency of Screen-Printed Silicon Solar Cells by Light-Induced Silver Plating. Photovoltaic Energy Conversion, Conference Record of the 2006 IEEE 4th World Conference on2006. p. 1056-9.

[44] Wanping C, Longtu L, Zhilun G. Effects of Electroless Nickel Plating on Resistivity-temperature Characteristics of (Ba1-xPbx)TiO3thermistor. Journal of Materials Research. 1997;12:877-9.

[45] Lee K, Fishwick PA. Building a model for real-time simulation. Future Generation Computer Systems. 2001;17:585-600.

[46] Henderson SG, Nelson BL. Chapter 1 Stochastic Computer Simulation. In: Shane GH, Barry LN, editors. Handbooks in Operations Research and Management Science: Elsevier; 2006. p. 1-18.

[47] Rinard IH. Core models, coordinators, and connectors in the dynamic modeling and simulation of multiphase systems. Computers & Chemical Engineering. 1996;20, Supplement 2:S969-S74.

[48] Altug Y, Wagner AB. Source and Channel Simulation Using Arbitrary Randomness. Information Theory, IEEE Transactions on. 2012;58:1345-60.

[49] Evstigneev IV, Schürger K. A limit theorem for random matrices with a multiparameter and its application to a stochastic model of a large economy. Stochastic Processes and their Applications. 1994;52:65-74.

[50] Tanaka H, Watada J. Possibilistic linear systems and their application to the linear regression model. Fuzzy Sets and Systems. 1988;27:275-89.

[51] Albrecht P. Parametric multiple regression risk models: Theory and statistical analysis. Insurance: Mathematics and Economics. 1983;2:49-66.

[52] Lai Y. Adaptive Monte Carlo methods for matrix equations with applications. Journal of Computational and Applied Mathematics. 2009;231:705-14.

[53] Li Y, Chiang H-D, Choi B-K, Chen Y-T, Huang D-H, Lauby MG. Load models for modeling dynamic behaviors of reactive loads: Evaluation and comparison. International Journal of Electrical Power & Energy Systems. 2008;30:497-503.

[54] Meinert TS, Don Taylor G, English JR. A modular simulation approach for automated material handling systems. Simulation Practice and Theory. 1999;7:15-30.

[55] Perissi I, Borri C, Caporali S, Lavacchi A. Current Density Simulations in the Electrodeposition from Ionic Liquids: Effects of the Conductivity. COMSOL Conference. Milan: COMSOL 2009.

[56] Obaid N, Sivakumaran R, Lui J, Okunade A, . Modelling the Electroplating of Hexavalent Chromium. COMSOL Conference. Boston2013.

[57] Strusevich N, Patel M, Bailey C. Parametric modeling study of basic electrodeposition in microvias. Electronic Materials and Packaging (EMAP), 2012 14th International Conference on2012. p. 1-5.

[58] Wei L, Haiyong C, Liming G, Ming L. Simulation of TSV copper electrodeposition process with additives. Electronic Packaging Technology (ICEPT), 2013 14th International Conference on2013. p. 480-4.

[59] Hughes M, Bailey C, McManus K. Multi Physics Modelling of the Electrodeposition Process. Thermal, Mechanical and Multi-Physics Simulation Experiments in Microelectronics and Micro-Systems, 2007 EuroSime 2007 International Conference on2007. p. 1-8.

[60] Griffiths SK, Nilson RH, Ting A, Bradshaw RW, Bonivert WD, Hruby JM. Modeling electrodeposition for LIGA microdevice fabrication. Microsystem Technologies. 1998;4:98-101.

[61] Son YJ, Wysk RA. Automatic simulation model generation for simulation-based, real-time shop floor control. Computers in Industry. 2001;45:291-308.

[62] Fan W. Simulation of queueing network with time varying arrival rates. Mathematics and Computers in Simulation. 1976;18:165-70.

[63] Czeczot J. Modelling for the effective control of the electric flow heaters – Simulation validation. Simulation Modelling Practice and Theory. 2008;16:429-44.

[64] Bergen SD, McGaughey RJ, Fridley JL. Data-driven simulation, dimensional accuracy and realism in a landscape visualization tool. Landscape and Urban Planning. 1998;40:283-93.

[65] Chen Y, Cai G, Wu Z. Modularization modeling and simulation of turbine test rig main test system. Applied Mathematical Modelling. 2011;35:5382-99.

[66] Markovitch NA, Profozich DM. Arena software tutorial. Proceedings of the 28th conference on Winter simulation. Coronado, California, USA: IEEE Computer Society; 1996. p. 437-40.

[67] Li Q, Ito K, Wu Z, Lowry CS, Loheide Ii SP. COMSOL Multiphysics: A Novel Approach to Ground Water Modeling. Ground Water. 2009;47:480-7.

[68] Piela PC, Epperly TG, Westerberg KM, Westerberg AW. ASCEND: an object-oriented computer environment for modeling and analysis: The modeling language. Computers & Chemical Engineering. 1991;15:53-72.

[69] Datta A, Rakesh V. An Introduction to Modeling of Transport Processes. In: Mark S. W. SC, editor.: Cambridge University Press; 2009.

[70] Wegener A, Hellbruck H, Fischer S, Schmidt C, Fekete S. AutoCast: An Adaptive Data Dissemination Protocol for Traffic Information Systems. Vehicular Technology Conference, 2007 VTC-2007 Fall 2007 IEEE 66th2007. p. 1947-51.

[71] Starinshak DP, Smith ND, Wilson JD. Using COMSOL Multiphysics software to model anisotropic dielectric and metamaterial effects in folded-waveguide traveling-wave tube slow-wave circuits. Vacuum Electronics Conference, 2008 IVEC 2008 IEEE International2008. p. 162-3.

[72] Green RA. Getting a handle on MATLAB graphics. Potentials, IEEE. 2007;26:31-7.

[73] Lowney JR, Larrabee RD. The use of Fick's law in modeling diffusion processes. Electron Devices, IEEE Transactions on. 1980;27:1795-8.

[74] Sanchez IC, DiMarzio EA. Dilute-Solution Theory of Polymer Crystal Growth. Some Thermodynamic and Predictive Aspects for Polyethylene. Macromolecules. 1971;4:677-87.

[75] Tao DP. Prediction of the thermodynamic properties of binary continuous solid solutions by infinite dilute activity coefficients. Thermochimica Acta. 2003;408:67-74.

[76] Noren DA, Hoffman MA. Clarifying the Butler–Volmer equation and related approximations for calculating activation losses in solid oxide fuel cell models. Journal of Power Sources. 2005;152:175-81.

[77] Dolati A, Afshar A, Ghasemi H. A kinetic study on the electrodeposition of cadmium with the presence of organic agents in sulfate solutions. Materials Chemistry and Physics. 2005;94:23-8.

[78] Miyazaki Y, Kajitani T. Preparation of Bi2Te3 films by electrodeposition. Journal of Crystal Growth. 2001;229:542-6.

[79] Martell AE. Entropy and the second law of thermodynamics. Journal of Chemical Education. 1946;23:166.

[80] Lu X. Application of the Nernst-Einstein equation to concrete. Cement and Concrete Research. 1997;27:293-302.

[81] Cai J, Jin C, Yang S, Chen Y. Logistic distributed activation energy model − Part 1: Derivation and numerical parametric study. Bioresource Technology. 2011;102:1556-61.

[82] Seyedi H, Abam Z, Golabi S. Comprehensive Analysis of the Impacts of Different Parameters on Transmission Line Switching Overvoltages. International Review on Modelling & Simulations. 2012;5:2174-82.

[83] Kamata M, Paku M. Exploring Faraday's Law of Electrolysis Using Zinc−Air Batteries with Current Regulative Diodes. Journal of Chemical Education. 2007;84:674.

[84] Haynes WM. CRC Handbook of Chemistry and Physics, 93rd Edition: Taylor & Francis; 2012.

[85] Yong H, Jing Z, Zhou Y. The critical current density in superconducting cylinder with different cross sections. Journal of Applied Physics. 2012;112:103913.

[86] Santos S, Bastardo J. Conductivity Studies of Poly(ethylene oxide)/Copper Sulfate Solid Solutions. International Journal of Polymeric Materials. 2005;54:415-25.

APPENDIX

APPENDIX A

MOLARITY OF THE SOLUTION

Molecular weight of $CuSO_4.5H_2O = 249.68\ g/mol$ (As on the bottle)

Number of moles = 18.8 $(Taken)/249.68$ =.0753 moles

H_2SO_4 used was 1N, which is equivalent to 2M solution

Solution of H_2SO_4 used was 7 ml

Number of moles = 2*.007=.014 moles

Total no of moles = .0753+.014 = .0893

Volume used = 100+7=107ml

Molarity of the solution = .0893*1000/100=.83M

APPENDIX B

MASS PERCENTAGE

Mass of $CuSO_4.5H_2O$ used was 18.8 g

Total mass percentage$= \dfrac{18.8}{18.8+100+98*2*.007} = 15.57\%$

Using the Electrical Conductivity of Aqueous Solutions from the Chemistry Handbook, based on

the mass percentage, the electrolyte conductivity of the solution was used.

ELECTRICAL CONDUCTIVITY OF AQUEOUS SOLUTIONS

The following table gives the electrical conductivity of aqueous solutions of some acids, bases, and salts as a function of concentration. All values refer to 20 °C. The conductivity κ (often called specific conductance in older literature) is the reciprocal of the resistivity. The molar conductivity Λ is related to this by Λ = κ/c, where c is the amount-of-substance concentration of the electrolyte. Thus if κ has units of millisiemens per centimeter (mS/cm), as in this table, and c is expressed in mol/L, then Λ has units of S cm² mol⁻¹. For these electrolytes the concentration c correspond-

ing to the mass percent values given here can be found in the table "Concentrative Properties of Aqueous Solutions" in Section 8.

References

1. CRC Handbook of Chemistry and Physics, 70th Edition, Weast, R. C., Ed., CRC Press, Boca Raton, FL, 1989, p. D-221.
2. Wolf, A. V., Aqueous Solutions and Body Fluids, Harper and Row, New York, 1966.

Electrical Conductivity κ in mS/cm for the Indicated Concentration in Mass Percent

Name	Formula	0.5%	1%	2%	5%	10%	15%	20%	25%	30%	40%	50%
Acetic acid	CH₃COOH	0.3	0.6	0.8	1.2	1.5	1.7	1.7	1.6	1.4	1.1	0.8
Ammonia	NH₃	0.5	0.7	1.0	1.1	1.0	0.7	0.5	0.4			
Ammonium chloride	NH₄Cl	10.5	20.4	40.3	95.3	180						
Ammonium sulfate	(NH₄)₂SO₄	7.4	14.2	25.7	57.4	105	147	185	215			
Barium chloride	BaCl₂	4.7	9.1	17.4	40.4	76.7	109.0	137.0				
Calcium chloride	CaCl₂	8.1	15.7	29.4	67.0	117	157	177	183	172	106	
Cesium chloride	CsCl	3.8	7.4	13.8	32.9	65.8	102	142				
Citric acid	H₃C(OH)(COO)₃	1.2	2.1	3.0	4.7	6.2	7.0	7.2	7.1			
Copper(II) sulfate	CuSO₄	2.9	5.4	9.3	19.0	32.2	42.3					
Formic acid	HCOOH	1.4	2.4	3.5	5.6	7.8	9.0	9.9	10.4	10.5	9.9	8.6
Hydrogen chloride	HCl	46.1	92.9	183								
Lithium chloride	LiCl	10.1	19.0	34.9	76.4	127	155	170	165	146		